Solid-state: Versus solution investigation of a luminescent chiral BINOL-derived bisphosphate single-molecule magnet

C.A. Mattei, V. Montigaud, Frédéric Gendron, S. Denis-Quanquin, V. Dorcet, N. Giraud, François Riobé, G. Argouarch, Olivier Maury, Boris Le Guennic, et al.

Solid-State *versus* Solution Investigation of a Luminescent Chiral BINOL-Derived Bisphosphate Single-Molecule Magnet

Carlo Andrea Mattei,[a] Vincent Montigaud,[a] Frédéric Gendron,[a] Sandrine Denis-Quanquin,[b] Vincent Dorcet,[a] Nicolas Giraud,[c] François Riobé,[b] Gilles Argouarch,[a] Olivier Maury,[b] Boris Le Guennic,*[a] Olivier Cador,[a] Claudia Lalli,[a] Fabrice Pointillart*[a]

[a] *Univ Rennes, CNRS, ISCR (Institut des Sciences Chimiques de Rennes) - UMR 6226, F-35000 Rennes, France. E-mail : fabrice.pointillart@univ-rennes1.fr*
[b] *Univ Lyon, ENS de Lyon, CNRS UMR 5182, Université Claude Bernard Lyon 1, Laboratoire de Chimie, F69342, Lyon, France.*
[c] *Université de paris, Laboratoire de Chimie et Biochimie Pharmacologies et Toxicologies, UMR CNRS 8601, Paris, France*

The enantiopure coordination polymer $[Dy(hfac)_3((\mathbf{\mathit{S/R}})\text{-L})]_n$ (**[(*S/R*)-1]$_n$**) involving a BINOL-derived bisphosphate ligand (***S/R*)-L** is reported. Paramagnetic NMR and computational investigations demonstrated the formation of mononuclear species **[(*S/R*)-1]** in CH_2Cl_2 solution and its optimized structure was determined. The experimental electronic circular dichroism signals of **(*S/R*)-L** were strongly enhanced after metal coordination **[(*S/R*)-1]**. Both polymeric and mononuclear structures displayed field-induced Single-Molecule Magnet (SMM) behaviour with similar multi-relaxation processes due to the retention of crystal-field splitting determined by CASSCF calculations and this despite the strong structural transformation between the two media. The HOMO→LUMO transition of the **(*S*)-L** ligand induced the classical Dy(III) emission at 77 K that was correlated with the magnetic properties. **[(*S*)-1]$_n$** is described as one-dimensional assembly of chiral luminescent Single-Ion Magnet (SIM).

Introduction

Since few decades, scientific communities have been investigating molecular materials because of their multiple physical properties especially when more than one is displayed in a unique system. Such system is called multifunctional or multiple-properties molecular material.[1-8] One of the most studied properties in molecular materials is probably chirality.[9-12] In fact chiral molecular materials display specific physical and chemical properties such as multiferroic effect, asymmetric catalysis…opening up the field of applications.[13-16] Moreover the combination of two properties such as chirality and magnetism, for example in chiral molecular magnets, can lead to the observation of a third property i.e. magneto-chiral anisotropy.[17-27]

Since the discovery in 2003 of the Single-Molecule Magnet (SMM) behaviour for a mononuclear complex of Tb(III),[28] the molecular magnetism field is dominated by the investigation of lanthanide-based SMMs.[29-37] SMMs are nanomagnets presenting blocking reversal magnetization up to 80 K[38] with great interest for potential applications in high density data storage.[39-40] At low temperature, SMMs are able to display quantum properties opening the doors to several other applications in molecular spintronics,[41-45] quantum computing[46-50] and magneto-optics.[51]

In addition, one of the advantages in using lanthanide ions is their specific luminescence which can be seen as a fingerprint of the ground level crystal-field splitting and thus can be correlated with magnetic properties.[52-65] Combining the two ingredients, luminescent lanthanides and chirality, multi-properties SMMs were recently reported such as luminescent chiral SMMs,[66] ferroelectric SMMs,[67-71] or magneto-chiral SMMs[72] but examples remain scarce. In these examples, the chirality mainly arises from the ligands which play crucial roles in the sensitization of the emission properties and for the optical activity. In order to optimize the latter properties, one strategy consists in using chiral ligand with an high optical activity and extended π-conjugated systems such as [n]-helicenes[73] and binaphthyl derivatives.[74] The formers were used by some of us to produce chiral SMMs[75-77] and singlet oxygen photosensitizers[78] while binaphthyl derivatives are well-known for enantioselective Diels-Alder reactions[79-84] and were recently described for Circularly Polarized Luminescence (CPL).[85-87]

In this article, enantiopure forms of the BINOL-derived bisphosphate **(*S/R*)-L** (Scheme 1) were used to link $Dy(hfac)_3$ units ($hfac^-$ = 1,1,1,5,5,5-hexafluoroacetylacetonate) to form the solid-state enantiopure coordination polymers of formula $[Dy(hfac)_3(\mathbf{(S/R)\text{-}L})]_n$, called here (**[(*S/R*)-1]$_n$**), whereas a monomeric form **[(S/R)-1]** was formed in solution. Deep magnetic and optical investigations were carried out showing 1D assembly of luminescent field-induced-SMM and Single-Ion Magnet (SIM) respectively in solid-state and solution. Coordination of the lanthanide units induced strong enhancement of the electronic circular dichroism contributions at low energy in solution.

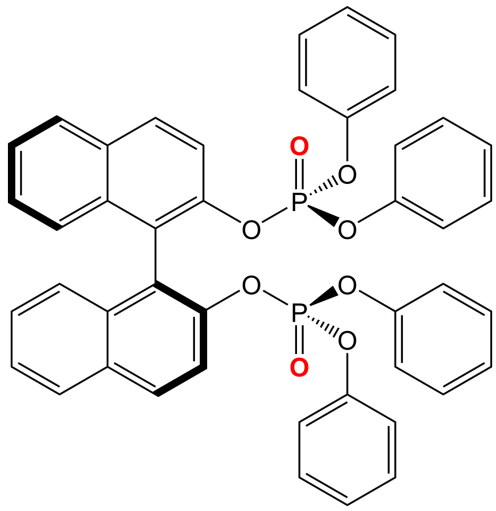

Chart 1. Molecular structure of the ligand **(*S*)-L**.

Experimental

The precursors $M(hfac)_3{\cdot}2H_2O$ ($hfac^-$ = 1,1,1,5,5,5-hexafluoroacetylacetonate anion)[88] and **(*S/R*)-L** ligand[89] were synthesized following previously reported methods. All the other reagents were purchased from Merck Co., Inc. and used without further purification.

Synthesis of the complex $[M(hfac)_3((S/R)\text{-L})]_n$ (M = Dy [(*S/R*)-1]$_n$, Eu [(*S/R*)-2]$_n$, Y [(*S/R*)-3]$_n$). 0.04 mmol of $M(hfac)_3{\cdot}2H_2O$ (32.8 mg for M = Dy, 29.8 mg for M = Y and 32.4 mg for M = Eu) were added into a solution of 30.0 mg of **(*S*)-L** or **(*R*)-L** (0.04 mmol) in 2 mL of CH_2Cl_2. After 15 minutes of stirring, 80 mL hexane were layered. After several days, the solution was slowly evaporated leading to a colorless and microcrystalline solid. Yield 56.4 mg (92 %) for **[(*S*)-1]$_n$**, 42.3 mg (69 %) for **[(*S*)-2]$_n$**, 43.9 mg (72 %) for **[(*S*)-3]$_n$**. Anal. Calcd (%) for $C_{59}H_{35}DyF_{18}O_{14}P_2$: C 46.15, H 2.28; found: C 46.09, H 2.39.; $C_{59}H_{35}EuF_{18}O_{14}P_2$: C 46.46, H 2.30; found: C 46.09, H 2.40. $C_{59}H_{35}YF_{18}O_{14}P_2$: C 48.47, H 2.40; found: C 49.01, H 2.44. I.R. (KBr, range 3200 – 400 cm^{-1}): 3136 (w), 3080 (w), 3068 (w), 2964 (w), 1656 (s), 1627 (w), 1591 (m), 1558 (m), 1526 (m), 1501 (s), 1489 (s), 1456 (w), 1432 (w), 1363 (w), 1348 (w), 1254 (s), 1191 (s), 1143 (s), 1102 (m), 1079 (m), 1029 (s), 1015 (s), 1005 (m), 994 (m), 961 (m), 951 (m), 902 (w), 875 (w), 869 (w), 850 (w), 821 (m), 807 (m), 796 (m), 779 (m), 763 (m), 753 (m), 740 (w), 704 (w), 686 (m), 662 (m), 615 (w), 585 (m), 558 (w), 554 (w), 526(w), 517 (w), 502(w), 495 (w), 482 (w), 464 (w) and 457 (w) cm^{-1}. For **[(*R*)-2]$_n$**, slow evaporation from CH_2Cl_2/hexane led to single crystals which were suitable for X-ray studies.

Materials and methods

Single crystal X-ray structure analysis. Single crystal of **[(*R*)-2]$_n$** was mounted on a APEXIII D8 VENTURE Bruker-AXS diffractometer for data collection (MoK_α radiation source, λ = 0.71073 Å), from the Centre de Diffractométrie (CDIFX), Université de Rennes 1, France. Structure was solved with a direct method using the SHELXT program[90] and refined with a full matrix least-squares method on F^2 using the SHELXL-14/7 program[91]. Crystallographic data are summarized in Table S1. Complete crystal structure results as a CIF file (CCDC 1980770) including bond lengths, angles, and atomic coordinates are deposited as Supporting Information.

Physical Measurements. The elementary analyses of the compounds were performed at the Centre Régional de Mesures Physiques de l'Ouest, Rennes. Absorption spectra were recorded on a JASCO V-650 spectrophotometer in diluted solution, using spectrophotometric grade solvents. Electronic circular dichroism (ECD) was measured on a Jasco J-815 Circular Dichroism Spectrometer (IFR140 facility – Biosit- Université de Rennes 1). Emission spectra were measured using Horiba-Jobin–Yvon Fluorolog-3 fluorimeter. The steady-state luminescence was excited by unpolarized light from a 450 W xenon continuous wave (CW) lamp and detected at an angle of 90° by using a Hamamatsu R928. For low temperature measurements, samples were placed in 4 mm quartz tubes and set into a quartz fill with liquid nitrogen. The magnetic susceptibility measurements were performed on solid polycrystalline samples immobilized in Teflon pellets to prevent any orientation of the crystallites with the magnetic field. The dc magnetic susceptibility measurements were performed with a Quantum Design MPMS-XL SQUID magnetometer between 2 and 300 K in applied magnetic field of 0.02 T for temperatures of 2-20 K, 0.2 T for temperature of 20-80 K and 1T for temperatures of 80-300 K. The ac magnetic susceptibility measurements were performed on a Quantum Design MPMS-XL SQUID for frequencies between 1 and 1000 Hz and a Quantum Design PPMS magnetometers for frequencies between 50 and 10000 Hz. These measurements were all corrected for the diamagnetic contribution as calculated with Pascal's constants.

NMR experiments. ^1H NMR spectra were acquired on a 400 MHz Bruker Avance III HD spectrometer equipped with a Nitrogen-cooled Prodigy cryoprobe. The ligands and the complexes were solubilized in $CDCl_3$. 3mm diameter NMR tubes were used to avoid convection issues (Figs. S4 and S5). All the chemical shifts are given in Table S5. Diffusion experiments were performed with a diffusion time Δ of 50 ms. Sine shaped pulse field gradients were used with a length δ of 1.5 ms and the gradient intensity was linearly incremented from 0.96 to 45.18 $G.cm^{-1}$ over 30 experiments (Fig. S6). The temperature was regulated at 298K. Diffusion curves were fitted using the Dynamics Centre software implemented in Topspin (Bruker). T_1 measurements were performed using the inversion recovery sequence. 16 K to 128K points were acquired for a spectral width of 14 to 200 ppm. The relaxation delay was set between 2 and 10 s. 8 or 10 experiments were recorded with a delay t varying between 10 ms and 1 or 10 s depending on the paramagnetism of the sample. ^{31}P NMR data were acquired on a 300MHz Bruker Advance III HD spectrometer equipped with a broadband BBFO probe. A pulse sequence with power-gated decoupling was used, with 128 scans, an acquisition time of 0.67 s and a relaxation delay of 2 s (Fig. S7).

Computational details. DFT geometry optimizations and TD-DFT excitation energy calculations of the ligand **(*S*)-L** were

carried out with the Gaussian 09 (revision A.02) package[92] employing the PBE0 hybrid functional.[94,103] All atoms were described with the SVP basis sets.[95] The first 50 monoelectronic excitations were calculated. In all steps, a modelling of bulk solvent effects (solvent = dichloromethane) was included through the Polarizable Continuum Model (PCM),[96] using a linear-response non-equilibrium approach for the TD-DFT step.[97,98]

The solution structures **[(*S/R*)-1**] were obtained using DFT calculations with the Amsterdam Density Functional (ADF) software package.[100-102] These calculations employed the hybrid functional PBE0[94,103] (Perdew-Burke-Ernzhof) containing 25 % of exact exchange in combination with the triple-ζ STO all-electron basis set with two polarization functions for all atoms (TZ2P)[104] and included scalar relativistic effects via the Zeroth-Order Relativistic Approximation (ZORA).[107] Solvent effects were taken into account by using the Conductor-Like Screening Model (COSMO)[108] with the dielectric constant of 4.8 to model chloroform. To avoid convergence issues, the paramagnetic Dy(III) ion was replaced by a diamagnetic Lu(III) ion for these structural optimizations.

The isotropic ^{1}H NMR chemical shifts were calculated with the NMR[110] module as implemented in ADF and are given with respect to the tetramethylsilane (TMS). In the case of the paramagnetic complex, the pseudo-contact shifts (δ^{PCS}) were calculated using the point-dipole approximation as follows:[111]

$$\delta^{PC}=\frac{1}{12\pi \mathbf{r}^3}\left[\Delta\chi_{ax}(3\cos^2\theta-1)+\frac{3}{2}\Delta\chi_{rh}\sin^2\theta\cos 2\phi\right]$$

in which ***r*** is the vector connecting the Dy(III) ion and the probed nucleus, $\Delta\chi_{ax}$ and $\Delta\chi_{rh}$ represent the axial and rhombic magnetic susceptibility anisotropy determined from the wavefunction theory calculations (see below), and θ and ϕ are the polar angles defining the position of the probed nucleus with respect to the frame of the magnetic susceptibility tensor. The wavefunction theory (WFT) calculations for the solid-state structures were realized on model complex of **[(*R*)-2]$_n$** (Fig. 1). The atomic positions were extracted from the X-ray crystal structure of **[(*R*)-2]$_n$** and only one Dy(III) ion was taken into account (n = 1). The optimization of the hydrogen and fluorine positions, while other atomic positions were kept frozen, have been carried out on the Y(III) parent molecule by Density Functional Theory (DFT) as implemented in the Gaussian 09 (revision D.01) package[92] using the PBE0 hybrid functional.[94,103] The « Stuttgart/Dresden » basis sets and effective core potentials were used to describe the yttrium atom[99] while other atoms were described with the SVP basis sets.[95] The WFT calculations were carried out with the help of the OpenMolcas software package.[112] In these calculations, the complete active space self-consistent field[113] (CASSCF) approach was used to treat the static correlation effects arising from the partially filled *4f* shell of the Dy(III) ion. The second-order Douglas-Kroll-Hess[114-117] scalar relativistic (SR) Hamiltonian was used to treat the scalar relativistic effects in combination with the all-electron atomic natural orbital relativistically contracted (ANO-RCC) basis set from the Molcas library.[118-120] The basis sets were contracted to the triple-ζ plus polarization (TZP) quality for the Dy, P and O atoms bonded to the lanthanide (Dy = 25s22p15d11f4g2h/8s7p4d3f2g1h; P = 17s12p5d4f2g/5s4p2d1f ; O = 14s9p5d3f2g/4s3p2d1f), and to the double-ζ quality for the rest of the O atoms and H, C and F atoms (H = 8s4p3d1f/2s ; C = 14s9p5d3f2g/3s2p, F = 14s9p5d3f2g/3s2p,). The calculations employed the state-averaged formalism at the SR level by taking into account the 21 sextet, the 224 quartet and the 490 doublet spin states arising from the 9 electrons spanning the seven 4f orbitals (i.e. CAS(9,7)). The spin-orbit coupling (SOC) was then introduced within a state interaction among the basis of calculated SR states using the restricted active space state interaction (RASSI) approach.[121] Herein the SOC matrix is diagonalized using the calculated 21 SR sextet, 224 SR quartet and the 98th lowest SR doublet spin states. The EPR *g*-factors were calculated according to Reference 122 as implemented in the RASSI module of OpenMolcas, whereas the magnetic susceptibility and magnetization calculations were performed using the Single-Aniso module of OpenMolcas as detailed in Reference 123. The dipole-dipole interaction[120] between two magnetic centers 1 and 2, bearing the magnetic moment μ_1 and μ_2 respectively, is described as

$$H_{dip} = -\frac{1}{R_{12}^3}\,\mu_1\cdot\,\mu_2 - 3(\mu_1\cdot\,\vec{r}_{12})(\mu_2\cdot\,\vec{r}_{12})$$

where R_{12} corresponds to the distance between the magnetic centers and $\vec{r}_{12}$ stands for the unit vector along the 12 direction.

Results and discussions

Structural description

[Eu(hfac)$_3$((*R*)-L)]$_n$ [(*R*)-2]$_n$: It crystallizes in the chiral orthorhombic space group C221 (N°20) (Table S1) and its asymmetric unit is composed of one **(*R*)-L** ligand and one Eu(hfac)$_3$ moiety. The Eu(hfac)$_3$ moieties are linked by the **(*R*)-L** ligands acting as a bridge through the two P=O groups to form a one-dimensional structure (Figs. 1 and S1). The Eu(III) ion is surrounded by eight oxygen atoms coming from three hfac$^-$ anions and two P=O groups coming from two different **(*R*)-L** ligands. The arrangement of the ligands around the central Eu(III) ion leads to a distorted square antiprism coordination polyhedron (D_{4d} symmetry, SAPR-8 = 0.300). The deviations from the ideal symmetries are determined by SHAPE[124] analysis (Table S2). The Eu-O_{hfac} bond lengths (2.395(9) Å) are found slightly longer than the Eu-$O_{P=O}$ bond lengths (2.372(9) Å). The $_{P=O}$O-Eu-$O_{P=O}$ angle is equal to 145.4(3)°. At this point, it could be important to precise that one of the two **L** ligands presents two disordered positions with 74/26 occupancies. The average angle value between the planes formed by the naphthyl groups is 100.9(2)°. The crystal packing (Figure S2) highlights both π-CH interactions and F···H contacts to ensure the cohesion of the crystal but no π-π stacking has been found. The shortest intra-chain Eu-Eu distance is equal to 12.65(2) Å while the shortest inter-chain Eu-Eu distance is determined in the same range with a value of 11.47(2) Å.

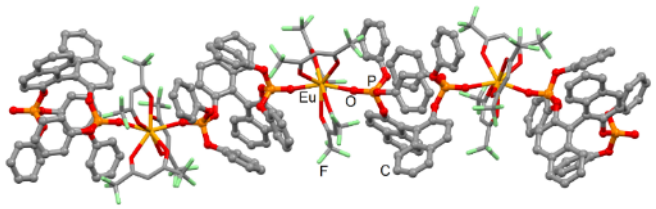

Fig. 1 Molecular structure of the one-dimensional polymer [Eu(hfac)$_3$((***R***)-L)]$_n$ **[(*R*)-2]$_n$**. Hydrogen atoms are omitted for clarity.

[Dy(hfac)$_3$((*S*)-L)]$_n$ [(*S*)-1]$_n$. No single crystals of satisfying quality for X-ray diffraction study could be obtained. Thus the phase purity for the Dy(III) analogue was checked by powder X-ray diffraction at room temperature. This study confirmed that the single crystal structure of **[(*R*)-2]$_n$** corresponds to the bulk material and its phase purity. Figure S3 displayed the excellent agreement between the experimental and simulated (from single crystal data) patterns allowing to conclude that **[(*S*)-1]$_n$** is pure and isomorphous to **[(*R*)-2]$_n$**.

NMR Studies

The significant solubility of the **[(*S/R*)-1]$_n$** derivative in classical organic solvents, prompted us to undertake a complete NMR study in order to definitively prove that the polymeric structure observed in the solid state was destroyed and replaced by smaller molecular weight oligomers or monomer as previously suggested but not fully demonstrated.[86] The ^{1}H NMR spectrum in $CDCl_3$ solution (Fig. 2) reveals a single set of 13 well resolved signals indicating that the solution structure retained a symmetry of the BINOL derivative (equivalence of naphthyl protons). The relaxation times (Table S3) are found to be rather short, in the range 1-80 ms, depending on the proximity of the proton to the strongly paramagnetic Dy(III) central ion. We have also evaluated the size of the molecular species in solution that resulted from the dissolution of the **[(*S/R*)-1]$_n$** derivatives, through the measurement of their diffusion coefficient. NMR experiments using pulsed gradient spin-echo (PGSE) are known as accurate tools to address this question. These methods have been recently successfully extended to paramagnetic species.[125] However, we recently demonstrated that paramagnetic complexes inducing too fast relaxation processes (T_1 < 10 ms) do not allow nuclear spin polarization to survive over typical diffusion delays inherent to the PGSE method.[126] To tackle this drawback the dysprosium derivative was bracketed by europium **[(*S*)-2]$_n$** and yttrium **[(*S*)-3]$_n$** analogous featuring larger and smaller ionic radius, respectively. Their NMR spectra (Fig. S4 and S5) indicate a similar behavior in solution and the relaxation times of the protons, in the range of 1-2 s for the diamagnetic Y(III) derivative and of 0.14-1.6 s for the weakly paramagnetic Eu(III) are now fully compatible with diffusion experiments (Table S4). The diffusion coefficients of the free ligand and the related Y(III) and Eu(III) complexes were measured (see experimental section for details) (Table 1) and allow us to estimate the size of the solution species thanks to eq (1):[127,128]

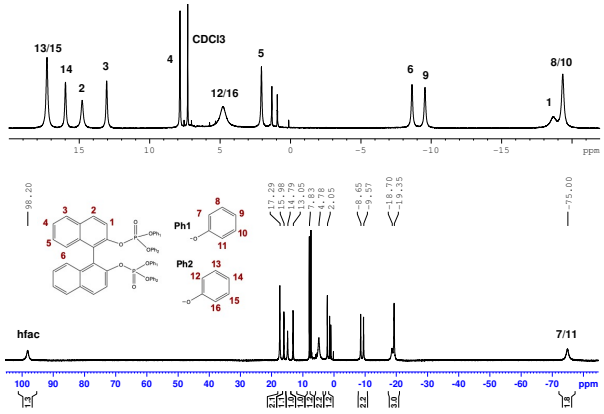

Fig. 2 (Bottom) Assigned ^{1}H NMR (400 MHz) spectrum of **[(*S*)-1]** in $CDCl_3$ at room temperature, with expansion of central region (top).

Table 1: Molecular weight (MW) and diffusion coefficients calculated according to eq(1) (D_{calc}) for the ligand **(*S*)-L** and for a monomer or a dimer, and measured by NMR (D_{obs}) for the ligand **(*S*)-L** and for the Europium and Yttrium complexes **[(*S*)-2]** and **[(*S*)-3]** in solution in $CDCl_3$.

	(*S*)-L	**[(*S*)-Ln]$_n$**					
		[(*S*)-1]) Ln = Dy		**[(*S*)-3]) Ln = Y**		**[(*S*)-2]) Ln = Eu**	
		n = 1	n = 2	n = 1	n = 2	n = 1	n = 2
MW	751	1534	3068	1461	2922	1524	3048
D_{calc} (µm^2.s^{-1})	753 *± 113*	544 *± 82*	405	557	414	547	406
D_{obs} (µm^2.s^{-1})	760 *± 8*	nd		673 ± 8		675 *± 8*	

$$(1) \qquad D = \frac{k_B T\left(\frac{3\alpha}{2}+\frac{1}{1+\alpha}\right)}{6\pi\eta\sqrt[3]{\frac{3MW}{4\pi\rho_{eff}N_A}}} \qquad \text{with } \alpha = \sqrt[3]{\frac{MW_S}{MW}}$$

where MW_s and MW represent the molecular weight of the solvent and the solute, respectively, η the viscosity of the solvent, k_BT the thermal driving force at a temperature T. The main hypothesis of this formula concerns the ρ_{eff} empirical parameter representing the effective density of an organic molecule, estimated to 619 kg.m^{-3}.[128] In the case of the free organic ligand **(*S*)-L**, a diffusion coefficient D_{obs} = 760 µm^2.s^{-1} was found in line with what is expected for a unique species with a molecular weight MW = 750 g.mol^{-1} leading to a calculated diffusion coefficient D_{calc} = 753 µm^2.s^{-1} according to eq(1) (Table 1). In the case of the complexes the experimental diffusion coefficient was measured to D_{obs} = 675 µm^2.s^{-1} for **[(*S*)-2]** (Figure S6) and D_{obs} = 673 µm^2.s^{-1} for **[(*S*)-3]**. As expected these values are lower than those of the free ligand because the molecular mass of the complexes are higher. However, these experimental diffusion coefficients are higher than a calculated one using eq(1) and the hypothesis of a monomer formation (Table 1). *A fortiori,* any larger oligomers (e.g. dimer in Table 1) will lead to even lower calculated diffusion coefficients and consequently the formation of a monomer in solution is the most probable scenario. Differences between the experimental and calculated diffusion coefficient values have already been described in the

literature and can be ascribed to the empirical effective density parameter determined in the case of organic molecules.[125] For coordination complexes containing heavy atoms especially in the cases of lanthanide ions, the ρ_{eff} parameter in eq(1) is expected to be largely underestimated, hence yielding underestimated calculated diffusion coefficient as is the case here. In conclusion, this NMR solution analysis suggests that the polymeric structure observed in the solid state is no longer conserved in solution and that a monomeric complex of formula **[M(hfac)$_3$((*S*)-L)]**, noted **[(*S*)-1,2,3]**, is formed, where **(*S*)-L** acts as a bidentate ligand. The complete assignment of the **[(*S*)-1]** ^{1}H NMR spectrum was then undertaken (Fig. 2). As the 2D COSY correlation and relaxation times (T_1) measurements were not sufficient for a full assignment, we decided first to study the NMR spectra obtained by dissolution of the europium **[(*S*)-2]** and yttrium **[(*S*)-3]** analogous in $CDCl_3$, having respectively a lower and no paramagnetism. Complete attribution was easily obtained for **[(*S*)-2,3]** thanks to 2D COSY and ^{13}C HSQC (Table S5). These data were used as a starting point to assign **[(*S*)-1]** using a comparative method (eq.2) described by Di Bari and co-workers to interpret the value of the experimentally measured shifts δ_i^{Exp}:[129]

$$\delta_i^{Exp}([Dy]) = \delta_i^{dia} + \mathrm{K} \times \delta_i^{PCS}([Eu]) \quad (2)$$

where δ_i^{dia} is the diamagnetic contribution determined by the spectrum of **[(*S*)-3]** and $\delta_i^{PCS}([Eu])$ represents the pseudo-contact shift contribution determined in the case of **[(*S*)-2]**. The assignment of **[(*S*)-1]** was checked by plotting the pseudo-contact shift contribution of **[(S)-1]** versus that of **[(*S*)-2]** leading to the expected linear relationship (Fig. S8). The complete assignments of **[(*S*)-1,2,3]** are given in Table S5. Thus, in the ^{1}H NMR spectrum of **[(*S*)-1]** the resonance at δ = 98.2 ppm can be unambiguously assigned to the three hfac$^-$ protons and the 12 remaining signals correspond to the ligand featuring an average two-fold symmetry in solution (12 signals are observed for 24 protons).

Starting from the hypothesis that such polymeric structure is transformed into a monomeric structure in solution,[86] DFT calculations were carried out in order to unravel the structure of such a monomer (see Computational details). The result of the optimized structure for the solution complex **[(*S*)-1]** is depicted on the top of Figure 3. To confirm the closeness of the calculated structure with respect to the experimental one, proton chemical shifts ($\delta^{Calc.}$) of the yttrium analogue and paramagnetic pseudo-contact shifts (δ^{PCS}) in the Dy-based complex were calculated and compared to the experimental values (see Tables S6 and S7). The calculated ^{1}H chemical shifts are found in good agreement with the experimental data for the diamagnetic Y(III) complex and confirm the presence of a 2-fold symmetry. In the paramagnetic Dy(III) complex, numerical agreement is not achieved with the experimental δ^{PCS}, which are strongly overestimated by the calculations and particularly for the phenyl groups of the ligand. However, the sign and relative magnitude between the shifts are reproduced when using the averaged values. For instance, the proton δ^{PCS} of the hfac$^-$ ligands are calculated at +109 ppm, while experimental shifts

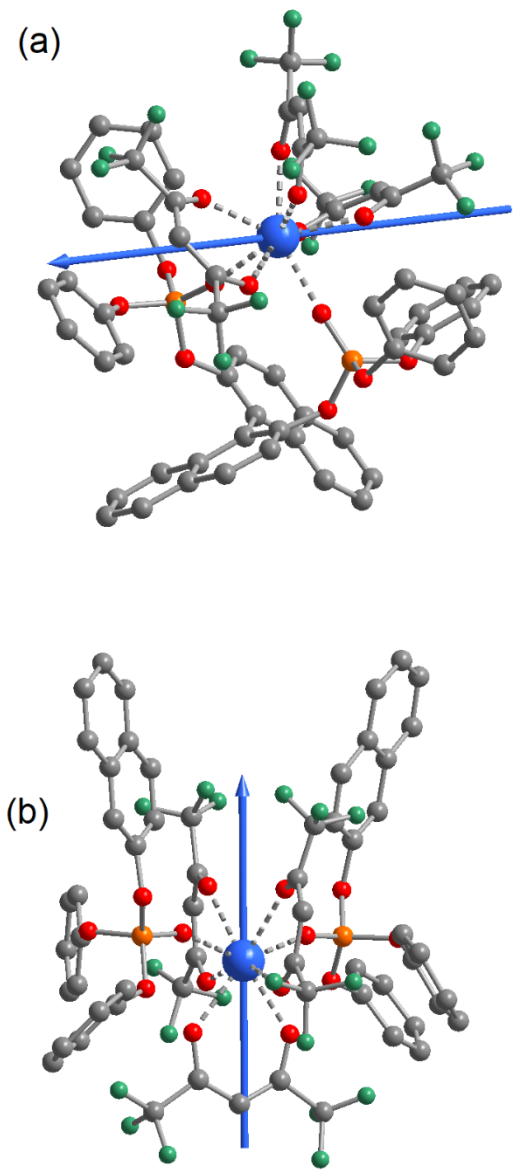

Fig. 3 (a) Optimized structure of **[(*S*)-1]$_n$** (n = 1) expected in CH_2Cl_2 solution and (b) the model used for quantum calculations in solid-state. Orientations of the principal magnetic axis computed for **[(*S*)-1]** (top) and **[(*S*)-1]$_n$** (bottom) are represented.

are measured at +92 ppm. The large deviations arise from the *static* picture of the calculation versus the *dynamic* picture of the measurements in solution. Indeed, as visible in Figure S9, the magnitude of the δ^{PCS} is strongly related to the magnetic anisotropy of the complex and the orientation of the molecule with respect to the magnetic axes. One can therefore conceive that the solution complex **[(*S*)-1]** exhibits free rotation of the phenyl groups, leading to averaged measured NMR values for these atoms.

Static magnetic properties

The experimental temperature dependence of $\chi_M T$ for **[(*S*)-1]$_n$** is represented on Figure 4. At room temperature $\chi_M T$ is equal to 13.91 cm^3 K mol^{-1} which is in good agreement with 14.17 cm^3 K mol^{-1} expected for the $^6H_{15/2}$ ground multiplet.[130] On cooling

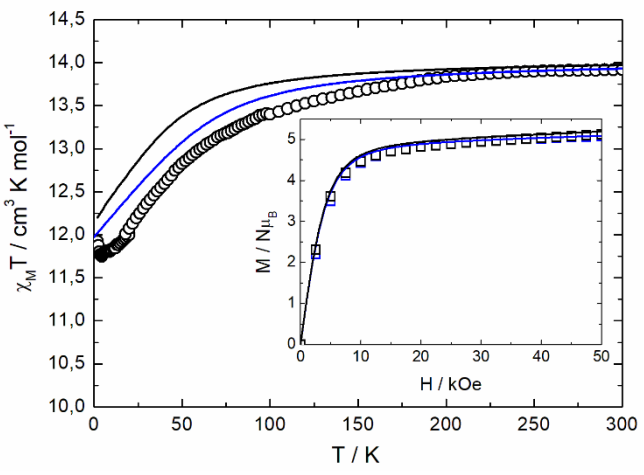

Fig. 4 Thermal dependence of $\chi_M T$ for **[(*S*)-1]$_n$** (solid-state measurements) (black circles). Inset: field variation of the magnetization measured at 2 K for **[(*S*)-1]$_n$** (solid-state measurements) (black squares) and **[(*S*)-1]** (CH_2Cl_2 C = 3×10^{-2} mol L^{-1} solution measurements) (blue squares). Black and blue lines correspond the ab initio computational results obtained with the solid-state and solution model compounds, respectively (see text for details).

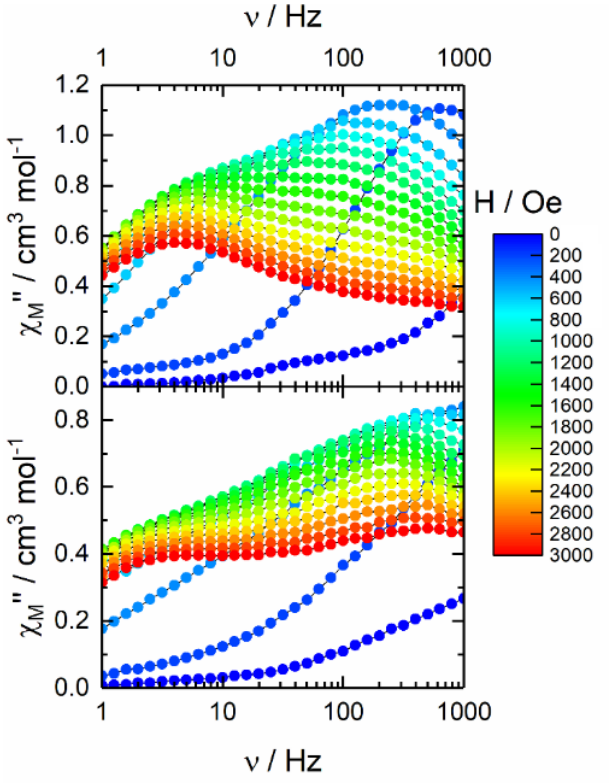

Fig. 5 Frequency dependence χ_M'' at 2 K in 0-3000 Oe field range for **[*S*-1]$_n$** (top) and **[(S)-1]** (frozen CH_2Cl_2 solution C = 3×10^{-2} mol L^{-1}, bottom).

down to 2 K, the thermal depopulation of the ligand field sublevels leads to a monotonic decrease of $\chi_M T$ which reaches 11.75 cm^3 K mol^{-1} at 4.5 K before showing a slight increase at the lowest temperatures. This increase below 4.5 K could be assigned to ferromagnetic dipolar interaction between the magnetic moment of the Dy(III) ions as already observed for other Dy(III) systems.[75] The field-dependence of magnetization measured at 2 K is depicted in inset of the Fig. 4. It shown classic behaviour for a Dy(III) ion in molecular systems. In fact, at 5 T, the value of the magnetization reaches 5.12 Nβ which is far from the expected saturated values of 10 Nβ for one Dy(III) in the absence of magnetic anisotropy but matches well with the stabilization of the M_J=±15/2 Kramers doublet (5 Nβ). The inset of Figure 4 depicted also the field-dependence of magnetization measured at 2 K for **[(*S*)-1]** (frozen CH_2Cl_2 solution) with similar behaviour than **[(S)-1]$_n$**.

Dynamic magnetic properties

The ac magnetic susceptibility for **[(*S*)-1]$_n$** was measured using the same immobilized crunched single crystals than for dc measurements while such measurements for **[(*S*)-1]** were done using a 0.03 M frozen CH_2Cl_2 solution of **[(*S*)-1]$_n$**. The out-of-phase component, χ_M'', of the ac susceptibility passes through a maximum at 7000 Hz at 2 K in zero external dc field for **[(*S*)-1]$_n$** (Fig. S10). Such maximum is shifted to higher frequencies with temperature and the relaxation time (τ) has been extracted with an extended Debye model (see SI, Fig. S11, Tables S8). The thermal dependence of the magnetic relaxation time in zero applied magnetic field was fitted taking into account the quantum tunnelling of the magnetization (QTM), and Raman processes ($\tau^{-1}=\tau_{TI}^{-1}+CT^n$).[131] The best fits were obtained considering the following parameters: C=34.6(5) $s^{-1}K^{-n}$ and n=4.23(79), τ_{TI} = 2.01(10)×10^{-5} s (Fig. S12). The normalized Cole-Cole plot shows that the out-of-phase component of the magnetic susceptibility represents 75 % of **[(*S*)-1]$_n$** at zero magnetic field (Fig. S13). The application of a constant magnetic field shifts the maximum of χ_M'' to lower frequency. Nevertheless, two contributions were observed as soon as the applied magnetic field value reached 500 Oe (Fig. 5 and S14) and the value of 1000 Oe was selected (value at which the two relaxation contributions are both at the lowest frequency and without saturation effects). At 1000 Oe, both in-phase, χ_M', and out-of-phase components of **[(*S*)-1]$_n$** show a frequency and temperature dependence (Figs. 6 and S15). The temperature dependence of the relaxation time of the magnetic susceptibility was extracted fitting simultaneously χ_M' and χ_M'' with an extended Debye model (Fig. S16). For the 2-3.5 K temperature range, the two contributions were taken into account while for T ≥ 4 K only one contribution was considered. The relaxation time of the magnetization (τ) for the low frequency (LF) contributions can be fitted using the thermally dependent Raman process ($\tau^{-1} = CT^n$) and Direct process (τ^{-1} = ATH^m with m fixed to 4) while the high frequency (HF) contribution could be fitted by a Direct process only. The best fits were obtained considering the following parameters: C=0.12(9) $s^{-1}K^{-n}$, n=6.10(48) and A = 8.87(36)×10^{-12} Oe^{-4} K^{-1} s^{-1} s for the LF contribution; A = 9.44(10)×10^{-10} Oe^{-4} K^{-1} $s^{-1}$for the HF contribution (Fig. 7). For H = 0 Oe the main magnetic relaxation process is the QTM with significant Raman contribution for T > 5.5 K (Fig. S12) while for H = 1000 Oe the main magnetic relaxation is the Raman with a Direct contribution for T < 2.5 K (Fig. S17). The LF and HF contributions could be attributed to Dy(III) ions in different coordination environment[132,133] or

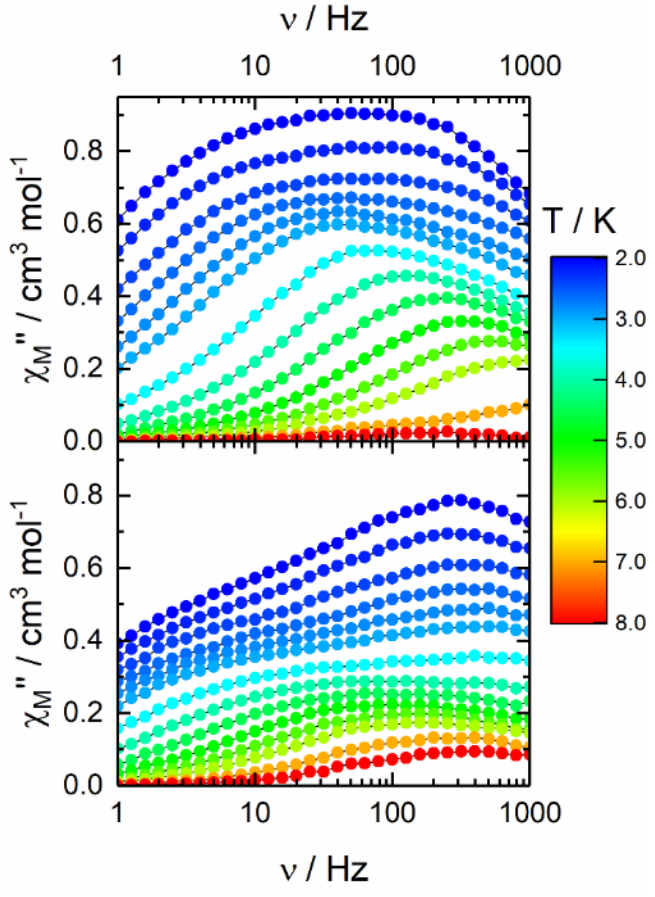

Fig. 6 Frequency dependence of χ_M'' between 2 and 8 K for **[(*S*)-1]$_n$** (above) and **[(*S*)-1]** (frozen CH_2Cl_2 solution C = 3×10^{-2} mol L^{-1}, below) under an applied magnetic field of 1000 Oe.

crystallographically independent Dy(III) ions[134] but also to the presence of significant dipolar interaction[135]. In the present case the pure phase of **[(*S*)-1]$_n$** involved only one Dy(III) centre and the frequency dependence of the magnetic susceptibility was performed at a field high enough to cancel the dipolar interaction. Thus the presence of both LF and HF contributions might be attributed to i) the structural disorder of one of the two coordinated ligands even if the second coordination sphere is affected[136,137] and ii) an intramolecular mechanism of multiple relaxation times at the single ion level because several relaxation modes might exist in the systems as demonstrated by L. F. Chibotaru and coll.[138]

To support the hypothesis of an intramolecular origin for the observation of multi-contributions of the magnetic susceptibility frequency dependence, a magnetic study in frozen CH_2Cl_2 solution was performed. Earlier in this paper, both NMR studies and DFT calculations concluded the presence of monomeric species in CH_2Cl_2 solution and the dissolution of a compound in an organic solvent is a well-known method to perform magnetic dilution leading to the cancelling of supramolecular[139] and dipolar interactions[140,141]. Scan field of the ac magnetic susceptibility for the isolated mononuclear specie **[(*S*)-1]** in solution shows somehow a similar behaviour than **[(*S*)-1]$_n$** and thus a 1000 Oe value was selected (Fig. 5 and S14) to study the ac magnetic properties of **[(*S*)-1]**. The frequency dependence of χ_M'' clearly shows two contributions (Figs. 6 and S15). The temperature dependence of the relaxation time was extracted using the same method than for **[(*S*)-1]$_n$** (Fig. S18). For the 2-3.5 K temperature range, the two contributions were taken into account while for $T \geq 4$ K only one contribution was considered. The relaxation time of the magnetization (τ) for the low frequency (LF) contributions can be fitted using the thermally dependent Raman process ($\tau^{-1} = CT^n$) and Direct process ($\tau^{-1} = ATH^m$ with m fixed to 4) while the high frequency (HF) contribution could be fitted by a Direct process only. The best fits were obtained considering the following parameters: C=0.15(15) $s^{-1}K^{-n}$, n=4.82(55) and A = $3.26(24)\times10^{-12}$ Oe^{-4} K^{-1} s^{-1} s for the LF contribution; A = $1.35(11)\times10^{-9}$ Oe^{-4} K^{-1} $s^{-1}$for the HF contribution (Fig. 7). The relaxation of the magnetization occurs through a Raman process with a Direct contribution for T < 2.5 K (Fig. S19). The observation of two different magnetic relaxations for **[(*S*)-1]** could not be attributed to different chemical magnetic centres or to significant intermolecular dipolar interactions[135] since only one type of mononuclear complex was found by the NMR study and the solution ac measurements prevent the strong interaction between the complexes. The absence of significant interaction between the molecules at C=3×10^{-2} mol L^{-1} was verified repeating the magnetic measurements at C=3×10^{-3} mol L^{-1} without any change. At this stage, such magnetic behaviour in frozen solution might be attributed to an intramolecular origin even in single-ion metal complexes as proposed for **[(*S*)-1]$_n$**.[138]

For the two compounds **[(*S*)-1]$_n$** and **[(*S*)-1],** the magnetization relaxed through Raman/Direct processes for the LF contribution and Direct process for the HF contribution. The difference might be imputed to the reorganization of the ligand around the metal centre and the matrix nature.

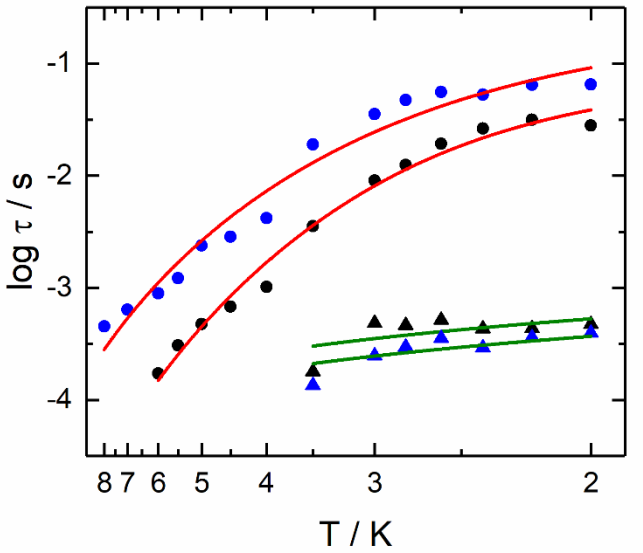

Fig. 7 Temperature dependences of the relaxation times (τ) at 1000 Oe for **[(*S*)-1]$_n$** (in black) and in the temperature range 2-6 K for the LF contribution (black dots) and 2-3.5 K for the HF contribution (black triangles) and for **[(*S*)-1]** in the temperature range 2-8 K for the LF contribution (blue dots) and 2-3.5 K for the HF contribution (blue triangles). Red and green lines are the best fitted curves with parameters given in the text.

Ab initio calculations

The experimental magnetic properties of both **[(*S*)-1]$_n$** and **[(*S*)-1]** were rationalized with the help of WFT calculations. The experimental thermal dependence $\chi_M T$ product and field dependence of the magnetization for **[(*S*)-1]$_n$** were well reproduced by the calculations (see Fig. 4). Interestingly, calculations performed on the model structure for the solution complex **[(*S*)-1]** revealed similar $\chi_M T$ product and magnetizations. As visible in Table S11, these similarities could arise from the presence of an analogous ground state (GS) in both cases, characterized by an almost pure $M_J = \pm 15/2$ (98 % and 97 % for **[(*S*)-1]$_n$** and **[(*S*)-1]** respectively), and by the combination of the energy splitting with the composition of the excited sates (ES) (Table S9). The experimental energy barrier values could be evaluated from the high temperature part of the log(τ) vs T curve (Fig. 7). The calculated gaps (30 cm^{-1} for **[(*S*)-1]$_n$** and 103 cm^{-1} for **[(*S*)-1]**) are higher than the experimental ones (16 cm^{-1} for **[(*S*)-1]$_n$** and 13 cm^{-1} for **[(*S*)-1]**). The discrepancy between computed and experimental values could be due to efficient under energy barrier relaxation processes such as Raman and Direct processes (Fig. S20). The two dysprosium centers present an almost uniaxial magnetic anisotropy (g_z = 19.70 and 19.57 for **[(*S*)-1]$_n$** and **[(*S*)-1]**, respectively). The main magnetic anisotropy axis appears perpendicular to the P=O-Dy-O=P direction and along the hfac$^-$ anion for **[(*S*)-1]$_n$**, while it was found perpendicular to the plane containing the two P=O groups for **[(*S*)-1]** i.e. for both cases along the most charged orientation of the oblate Dy(III) ion coordination sphere (Fig. 3). The structural disorder located on the bridging phosphate moieties was then studied by considering the configuration with the lowest occupancy coefficients, **[(*S*)-1]$_n$'** (Fig. S21)**.** In this configuration, the derived phosphate ligand and the close CF_3 groups are tilted. However, the small impact of the reorientation of the ligand upon the first coordination sphere geometry lead to almost no difference between **[(*S*)-1]$_n$'** and **[(*S*)-1]$_n$** in terms of ground state properties and crystal field splitting of the $^6H_{15/2}$ multiplet of the Dy(III) ion (Fig. S22 and Table S11). Consequently the two thermal dependences of the magnetic susceptibility are superimposed (Fig. S23). Moreover an evaluation of the dipolar interactions was done assuming an ising-type anisotropy (only the g_{zz} was considered). The results of such calculations have shown that the main dipolar interactions are of ferromagnetic nature along the a and c axis and of weaker antiferromagnetic nature along the b axis (Fig. S24). The average dipolar interactions are thus of ferromagnetic nature ($zJ' = 0.04$ cm^{-1}) in agreement with the increase of $\chi_M T(T)$ curve observed at low temperature (Fig. 4). Therefore, the origin of the two relaxation contributions observed in the solid-state cannot be attributed to the disorder of the ligands and might be attributed to intramolecular mechanisms. These computational results as well as the ac measurements highlighted that the non-significant *trans* versus *cis* position of the P=O anchoring groups might be due to the weaker participation of the oxygen atoms of the P=O than those of the hfac$^-$ anions to the crystal field and to the nature of the ground state.[142] The difference of Ln-O bond lengths and the charge on the first neighboring atoms have antagonist effect on the magnetic properties. Nevertheless, even if the Ln-$O_{P=O}$ distances are found shorter than the Ln-O_{hfac} bond lengths, the negatively charged character of the hfac$^-$ gets the best of the difference of bond lengths.

Photo-physical properties

Absorption and Electronic Circular Dichroism (ECD). The UV-visible absorption properties of **(*S*)-L**, **(*R*)-L**, **[(*S*)-1]** and **[(*R*)-1]** were studied in a CH_2Cl_2 solution (Fig. 8). Rationalization by TD-DFT calculations was performed. The experimental absorption spectra for both enantiopure free ligands are superimposed and they can be decomposed in four contributions localized at 31000, 34500, 38200 and 43000 cm^{-1} and respectively calculated at 32804, 36001, 41387 and 45568 cm^{-1} (Table S12). The lowest-energy excitation was attributed to the HOMO→LUMO transition, the two intermediate excitations were attributed to transitions involving mainly the HOMO and HOMO-1 to the LUMO, LUMO+1, LUMO+2 and LUMO+4. Finally the highest-energy excitation was attributed to π-π* transitions of the binaphthyl moieties (HOMO-1→LUMO+6/+7). The experimental absorption spectra for complexes are similar to those for free ligands except that an additional intense excitation appeared at 33000 cm^{-1} due to the π-π* transitions

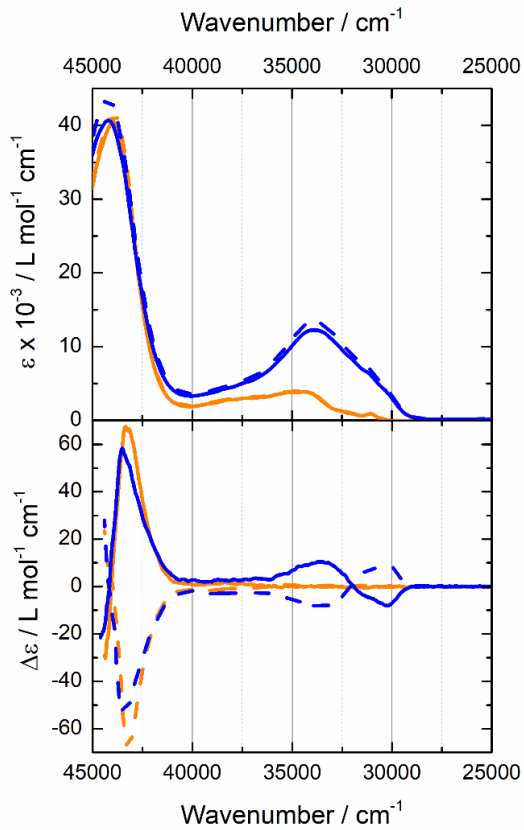

Fig. 8 (Top) Experimental UV-visible absorption spectra of **(*S*)-L** (orange line), **(*R*)-L** (dashed orange line), **[(*S*)-1]** (blue line) and **[(*R*)-1]** (dashed blue line) in CH_2Cl_2 solution (C = 5×10^{-5} mol.L^{-1}). (Bottom) Experimental ECD spectra of enantiopure **(*S*)-L** (orange line) and **(*R*)-L** (dashed orange line) (CH_2Cl_2, ca. 5×10^{-5} M) and respective Dy(III) complexes **[(*S*)-1]** (blue line) and **[(*R*)-1]** (dashed blue line) (CH_2Cl_2, ca. 5×10^{-5} M).

of the hfac⁻ anions.[143] CH_2Cl_2 solution-state circular dichroism measurements performed at room temperature for **(*S*)-L** and **(*R*)-L** confirmed their enantiomeric nature (Fig. 8). Cotton effect is very weak in the low-energy range while it is strong at high-energy range and dichroic contributions of opposite signs were observed at 38500 cm^{-1} and 42700 cm^{-1} for each enantiomer on the mirror-symmetrical dichroism spectra (Fig. 8). Such contributions come from the excitonic coupling between the π-π^* transitions of the naphthyl groups.[144-146] The ECD spectra for complexes highlighted a significant enhancement of the low-energy contributions centered at 30200 cm^{-1} and 33600 cm^{-1} while those at higher energy did not change. These observations might be due to the structural change induced by the coordination of the $Dy(hfac)_3$ unit, especially to the modification of the torsion angle of the binaphthyl group which mainly affect the low energy transitions. Indeed it was previously demonstrated that the optical activity of the binaphthyl-based ligands depends of the angle between the two planes formed by the naphthyl moieties.[147-150] The structural changes after coordination reaction are supported by the optical activity values (c 1.0, $CHCl_3$) for **(*S*)-L** ($[\alpha]_D^{25}$ = +1.2° cm^2 $dmol^{-1}$) and **(*R*)-L** ($[\alpha]_D^{25}$ = -1.0° cm^2 $dmol^{-1}$) which have been determined lower than those for **[(*S*)-1]** and **[(R)-1]** ($[\alpha]_D^{25}$ = ± 25.8° cm^2 $dmol^{-1}$).

Luminescence. Emission properties were first checked in both solution **[(*S*)-2]** and solid-state **[(*S*)-2]$_n$** for the ***S*** enantiomer of the Europium analogue at room temperature (Fig. S23). The excitation of the samples at 28570 cm^{-1} (350 nm) induced the characteristic Eu(III) ion-centered luminescence profile with five $^5D_0 \rightarrow {}^7F_J$ (J=0-4) and four (J=1-4) transitions respectively in solution and solid. The single Gaussian shape of the $^5D_0 \rightarrow {}^7F_J$ transition in solution is an additional indication of the presence of one specie in CH_2Cl_2 solution. In the case of europium, the splitting of each $^5D_0 \rightarrow {}^7F_J$ transition is correlated to the crystal field and is, therefore, representative of the local symmetry. The splitting of the $^5D_0 \rightarrow {}^7F_2$ transition in three is in agreement with the D_{4d} local symmetry of the europium coordination sphere.[151] Emission properties for the ***S*** enantiomer of the dysprosium complex were also studied in solution on **[(*S*)-1]** and solid-state on **[(*S*)-1]$_n$** at room temperature (Fig. S24) and low temperature. The excitation of the samples at 28570 cm^{-1} (350 nm) induced the characteristic Dy(III) ion-centered luminescence assigned to the $^4F_{9/2} \rightarrow {}^6H_J$ emission (J ranging from 9/2 to 15/2) (Fig. S26). The emission spectrum of **[(*S*)-1]$_n$** is more resolved than the one for **[(*S*)-1]** as commonly observed for molecular complexes. Looking at the magnetic properties, a zoom of the transition involving the $^6H_{15/2}$ ground state is shown in inset of the Figure S25. The total $^4F_{9/2} \rightarrow {}^6H_{15/2}$ emission range for **[(*S*)-1]** and **[(*S*)-1]$_n$** are very similar in agreement with the calculated energy splitting of the multiplet ground state (see ab initio calculations section). The difference could be attributed to the reorganization of the **S-L** and hfac⁻ ligands in solution.[152,153] It is now well-known that the highest-energy emission can be described as a photography of the ground state energy splitting which is at the origin of the magnetic properties of the single ion.[56,61,65] Thus the following discussion is focused on the solid-state measurements in order to have the best resolved spectra as possible. The top of the Figure 9 depicts the excitation (red line) and emission spectrum at 77 K (green line) of **[(*S*)-1]$_n$**. A simple Boltzmann population calculation starting from the experimental excitation spectrum supported the fact that at 77 K some of the excited states of the $^7F_{9/2}$ and $^6H_{15/2}$ levels are populated (Fig. S26) supporting the observation of "hot bands" for both excitation and emission spectra (Fig. 9). The calculation at the CASSCF level gave the energy splitting for the $^6H_{15/2}$ ground multiplet (green sticks on Fig. 9) and the $^4F_{9/2}$ excited multiplet (red sticks on Fig. 9). The experimental splitting the $^6H_{15/2}$ ground multiplet appears strongly underestimated by the calculations. The energy gap between the ground and first excited states of the $^6H_{15/2}$ crystal field splitting is 40 cm^{-1} which is in agreement with the energy barrier determined from the ab initio calculations (30 cm^{-1}) (Table S11). The value of 40 cm^{-1} is confirmed by the overlay with the excitation spectrum ("zero-phonon" transition) and the energy difference with the corresponding hot band (Fig. 9).

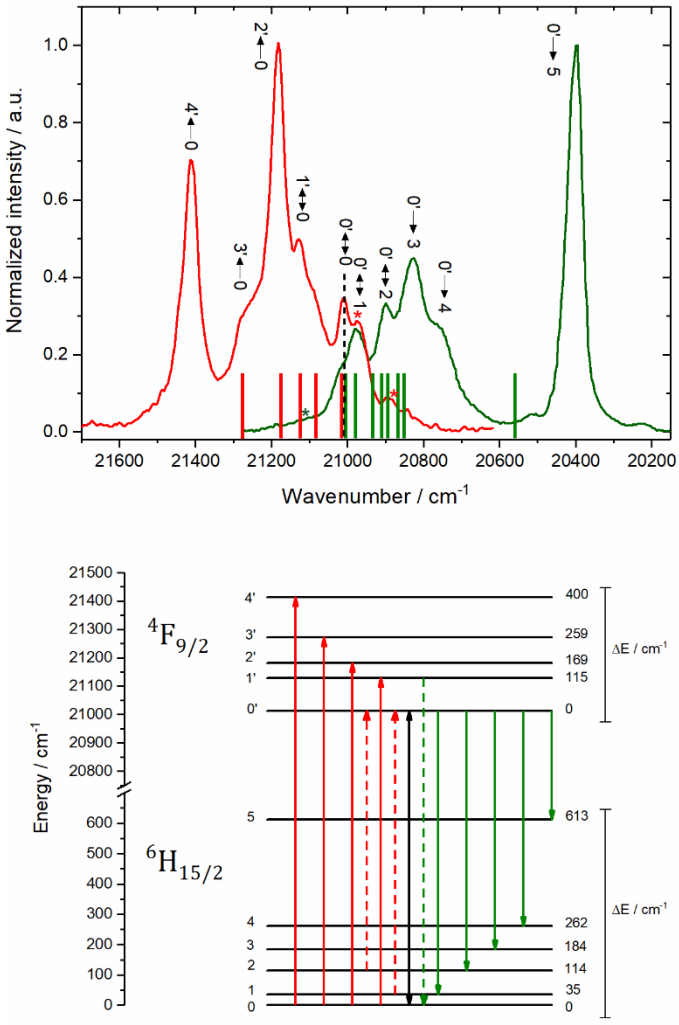

Fig. 9 (top) Excitation spectrum (red line) and emission spectra (green line) at 77 K of **[(*S*)-1]$_n$** with the calculated energy splitting for the $^4F_{9/2}$ (vertical red sticks) and $^6H_{15/2}$ (vertical green sticks) levels for an irradiation energy of 28570 cm^{-1}. "zero-phonon" transition is represented as black dashed line while the hot bands are indicated by stars. (bottom) Experimental energy diagram with related transitions. "Hot bands" are depicted in dashed lines.

Conclusions

Two pure enantiomers of dysprosium BINOL-derived bisphosphate $[Dy(hfac)_3(\textbf{\textit{S/R}}\text{-L})]_n$ (**[(*S/R*)-1]$_n$**) with polymeric structures are reported. The combination of both NMR and computational investigations concluded to the structural reorganization from a polymeric to a mononuclear **[(*S*)-1]** structure once **[(*S*)-1]$_n$** is in CH_2Cl_2 solution. Both species highlighted single-molecule magnet behavior under a 1000 Oe applied field through two Raman and Direct thermally dependent magnetic relaxation processes. The combination of the persistence of the multi-relaxation mechanism for the mononuclear species in solution and the computational results are strong indications of its intramolecular origin. The drastic structural modification between solid-state and solution induced only small magnetic changes because the crystal field kept the Ising character of the Dy(III) centre in both structures as confirmed by ab initio calculations. The EDC of **[(*S*)-1]** highlighted an enhancement of the optical activity in the low energy range after coordination of the $Dy(hfac)_3$ unit, due to the sensibility of the corresponding excitations of the binaphthyl torsion angle. Both **[(*S*)-1]$_n$** and **[(*S*)-1]** displayed dysprosium-centered emission under irradiation of the HOMO→LUMO excitation of the BINOL derived bisphosphate organic chromophore. The luminescence data at 77 K for **[(*S*)-1]$_n$** could be correlated to the experimental and calculated magnetic data. The present chiral luminescent single-molecule magnet opens the way to a rational investigation of the nature of the chiral ligand on the combined magnetic and optical properties such as single-molecule magnet and circularly polarized luminescence.

Conflicts of interest

There are no conflicts to declare.

Acknowledgements

This work was supported by CNRS, Université de Rennes and the European Research Council through the ERC-CoG 725184 MULTIPROSMM (project n. 725184). B.L.G., F.G. and V.M. thank the French GENCI/IDRIS-CINES center for high-performance computing resources. F.G. acknowledges Région Bretagne for a Stratégie d'Atractivité Durable Grant (SA18006-LnCPLSMM). Part of this work has been performed using the Spectroscopies-DCTP core facility (UMS Biosit, Université de Rennes 1- Campus de Villejean- 35043 RENNES Cedex, FRANCE).

Notes and references

1 E. Coronado, A. Forment-Aliaga, J. R. Galán-Mascarós, C. Giménez-Saiz, C. J. Gómez-Garcia, E. Martinéz-Ferrero, A. Nuez and F. M. Romero, Multifunctional molecular materials. *Solid State Sci.,* 2003, **5**, 917–924.

2 E. Coronado, C. Giménez-Saiz and C. Martí-Gastaldo, "Crystal engineering of multifunctional molecular materials," in Engineering of Crystalline Materials Properties, in NATO Science for Peace and Security Series B: Physics and Biophysics, eds J. J. Novoa, D. Braga and L. Addadi (Dordrecht: Springer), 2008, 173–191.

3 E. Coronado, F. Palacio and J. Veciana, Molecule-Based Magnetic Materials. *Angew. Chemie,* 2003, **42**, 2570–2572.

4 P. Gómez-Romero and C. Sánchez, Functional Hybrids Materials. Weinheim: Wiley-VCH 2004.

5 A. Fahmi, T. Pietsch, C. Mendoza and N. Cheval, Functional hybrid materials. *Mater. Today*, 2009, **12**, 44–50.

6 J. Rocha, L. D. Carlos, F. A. A. Paz and D. Ananias, Luminescent progress in hybrid materials science. *Chem. Soc. Rev.,* 2011, **40**, 926–940.

7 C. Sanchez, K. J. Shea and S. Kitagawa, Recent progress in hybrid materials science. *Chem. Soc. Rev.,* 2011, **40**, 471–472.

8 L. Ouahab, Multifunctional Molecular Materials. New York, NY: Taylor and Francis Group CRC Press 2012.

9 R. A. Garoff, E. A. Litzinger, R. E. Connor, I. Fishman and B. A. Armitage, Helical Aggregation of Cyanine Dyes on DNA Templates: Effect of Dye Structure on Formation of Homo- and Heteroaggregates. *Langmuir*, 2002, **18**, 6330–6337.

10 M. Wang, G. L. Silva and B. A. Armitage, DNA-Templated Formation of a Helical Cyanine Dye J-Aggregate. *J. Am. Chem. Soc.*, 2000, **122**, 9977–9986.

11 R. F. Pasternack, A. Giannetto, P. Pagano and E. J. Gibbs, Self-assembly of porphyrins on nucleic acids and polypeptides *J. Am. Chem. Soc.*, 1991, **113**, 7799–7780.

12 K. C. Hannah and B. A. Armitage, DNA-Templated Assembly of Helical Cyanine Dye Aggregates: A Supramolecular Chain Polymerization. *Acc. Chem. Res.*, 2004, **37**, 845–853.

13 Q.-H. Xia, H.-Q. Ge, C.-P. Ye, Z.-M. Liu and K.-X. Su, Advances in Homogeneous and Heterogeneous Catalytic Asymmetric Epoxidation. *Chem. Rev.*, 2005, **105**, 1603–1662.

14 W. Eerenstein, N. D. Mathur and J. F. Scott, Multiferroic and magnetoelectric materials. *Nature*, 2006, **442**, 759–765.

15 J. Chin, S. S. Lee, K. J. Lee, S. Park and D. H. Kim, A metal complex that binds α-amino acids with high and predictable stereospecificity. *Nature*, 1999, **401**, 254–257.

16 G. L. J. A. Rikken and E. Raupach, Enantioselective magnetochiral photochemistry. *Nature*, 2000, **405**, 932–935.

17 M. P. Groenewege, A theory of magneto-optical rotation in diamagnetic molecules of low symmetry. *Mol. Phys.*, 1962, **5**, 541–563.

18 G. Wagnière and A. Meier, The influence of a static magnetic field on the absorption coefficient of a chiral molecule. *Chem. Phys. Lett.*, 1982, **93**, 78–81.

19 L. D. Barron and J. Vrbancich, Magneto-chiral birefringence and dichroism. *Mol. Phys.*, 1984, **51**, 715–730.

20 J. L. J. A. Rikken and E. Raupach, Observation of magneto-chiral dichroism. *Nature*, 1997, **390**, 493–494.

21 L. D. Barron, Chirality, magnetism and light. *Nature*, 2000, **405**, 895–896.

22 C. Train, R. Gheorghe, V. Krstic, L. Chamoreau, N. S. Ovnesyan, G. L. J. A. Rikken, M. Gruselle and M. Verdaguer, Strong magneto-chiral dichroism in enantiopure chiral ferromagnets. *Nat. Mater.*, 2008, **7**, 729–734.

23 G. L. J. A. Rikken and E. Raupach, Pure and cascaded magnetochiral anisotropy in optical absorption. *Phys. Rev. E: Stat. Phys., Plasmas, Fluids, Relat. Interdiscip. Top.,* 1998, **58**, 5081–5084.

24 C. Koerdt, G. Duchs and G. L. J. A. Rikken, Magnetochiral Anisotropy in Bragg Scattering. *Phys. Rev. Lett.*, 2003, **91**, 073902.

25 Y. Kitagawa, H. Segawa and K. Ishii, Magneto-Chiral Dichroism of Organic Compounds. *Angew. Chem.*, 2011, **123**, 9299–9302.

26 Y. Kitagawa, T. Miyatakeb and K. Ishii, Evidence for atomic mixingvia multiple intermediates during the dynamic interconversion of silicate oligomers in solution. *Chem. Commun.*, 2012, **48**, 5091–5093.

27 S. Bordács, I. Kézsmárki, D. Szaller, L. Demkó, N. Kida, H. Murakawa and Y. Onose, Chirality of matter shows up via spin excitations. *Nat. Phys.*, 2012, **8**, 734–738.
28 N. Ishikawa, M. Sugita, T. Ishikawa, S. Y. Koshihara and Y. Kaizu, Lanthanide Double-Decker Complexes Functioning as Magnets at the Single-Molecular Level. *J. Am. Chem. Soc.*, 2003, **125**, 8694-8695.
29 R. Sessoli and A. K. Powell, Strategies towards single molecule magnets based on lanthanide ions. *Coord. Chem. Rev.*, 2009, **253**, 2328–2341.
30 F. Habib and M. Murugesu, Lessons learned from dinuclear lanthanide nano-magnets. *Chem. Soc. Rev.*, 2013, **42**, 3278–3288.
31 D. N. Woodruff, R. E. P. Winpenny and R. A. Layfield, Lanthanide Single-Molecule Magnets. *Chem. Rev.*, 2013, **113**, 5110–5148.
32 R. A. Layfield and M. Murugesu, Lanthanides and Actinides in Molecular Magnetism.Weinheim,Wiley-VCH 2015.
33 S. T. Liddle and J. van Slageren, Improving f-element single molecule magnets. *Chem. Soc. Rev.*, 2015, **44**, 6655–6669.
34 J. Tang and P. Zhang, Lanthanide Single Molecule Magnets. Berlin; Heidelberg: Springer-Verlag. 2015.
35 K. L. M. Harriman and M. Murugesu, An Organolanthanide Building Block Approach to Single-Molecule Magnets. *Acc. Chem. Res*. 2016, **49**, 1158–1167.
36 F. Pointillart, O. Cador, B. Le Guennic and L. Ouahab, Uncommon lanthanide ions in purely 4f Single Molecule Magnets. *Coord. Chem. Rev.*, 2017, **346**, 150-175.
37 F.-S. Guo, A. K. Bar and R. A. Layfield, Main Group Chemistry at the Interface with Molecular Magnetism. *Chem. Rev.*, 2019, **119**, 14, 8479-8505.
38 F.-S. Guo, B.-M. Day, Y.-C. Chen, M.-L. Tong, A. Mansikkamäki and R. A. Layfield, Magnetic hysteresis up to 80 kelvin in a dysprosium metallocene single-molecule magnet. *Science*, 2018, **362**, 1400-1403.
39 M. Mannini, F. Pineider, P. Sainctavit, C. Danieli, E. Otero, C. Sciancalepore, A. M. Talarico, M.-A. Arrio, A. Cornia, D. Gatteschi and R. Sessoli, Magnetic memory of a single-molecule quantum magnet wired to a gold surface. *Nat. Mater.*, 2009, **8**, 194-197.
40 M. Affronte, Molecular nanomagnets for information technologies. *J. Mater. Chem.* 2009, **19**, 1731–1737.
41 K. S. Pedersen, A.-M. Ariciu, S. McAdams, H. Weihe, J. Bendix, F. Tuna and S. Piligkos, Toward Molecular 4f Single-Ion Magnet Qubits. *J. Am. Chem. Soc.*, 2016, **138**, 5801-5804.
42 L. Bogani and W. Wernsdorfer, Molecular spintronics using single-molecule magnets. *Nat. Mater.*, 2008, **7**, 179–186.
43 R. Vincent, S. Klyatskaya, M. Ruben, W. Wernsdorfer and F. Balestro, Electronic read-out of a single nuclear spin using a molecular spin transistor. *Nature*, 2012, **488**, 357–360.
44 M. Ganzhorn, S. Klyatskaya, M. Ruben and W. Wernsdorfer, Strong spin–phonon coupling between a single-molecule magnet and a carbon nanotube nanoelectromechanical system. *Nat. Nano.*, 2013, **8**, 165–169.
45 A. Cornia and P. Seneor, The molecular way. *Nat. Mater.*, 2017, **16**, 505–506.
46 S. Thiele, F. Balestro, R. Ballou, S. Klyatskaya, M. Ruben and W. Wernsdorfer, Electrically driven nuclear spin resonance in single-molecule magnets. *Science*, 2014, **344**, 1135-1138.
47 M. N. Leuenberger and D. Loss, Quantum computing in molecular magnets. *Nature*, 2001, **410**, 789–793.
48 A. Ardavan, O. Rival, J. J. L. Morton, S. J. Blundell, A. M. Tyryshkin, G. A. Timco and R. E. P. Winpenny, Will Spin-Relaxation Times in Molecular Magnets Permit Quantum Information Processing? *Phys. Rev. Lett*., 2007, **98**, 057201.
49 P. C. E. Stamp and A. Gaita-Ariño, Spin-based quantum computers made by chemistry: hows and whys. *J. Mater. Chem*., 2009, **19**, 1718–1730.
50 M. J. Martínez-Pérez, S. Cardona-Serra, C. Schlegel, F. Moro, P. J. Alonso, H. Prima-García, J. M. Clemente-Juan, M. Evangelisti, A. Gaita-Arino, J. Sesé, J. Van Slagaren, E. Coronado and F. Luis, Gd-Based Single-Ion Magnets with Tunable Magnetic Anisotropy: Molecular Design of Spin Qubits. *Phys. Rev. Lett.*, 2012, **108**, 247213.
51 R. Sessoli, M.-E. Boulon, A. Caneschi, M. Mannini, L. Poggini, F. Wilhelm and A. Rogalev, Strong magneto-chiral dichroism in a paramagnetic molecular helix observed by hard X-rays. *Nat. Phys.*, 2015, **11**, 69–74.
52 M.-E., Boulon, G. Cucinotta, J. Luzon, C. Degl'Innocenti, M. Perfetti, K. Bernot, G. Calvez, A. Caneschi and R. Sessoli, Magnetic Anisotropy and Spin-Parity Effect Along the Series of Lanthanide Complexes with DOTA. *Angew. Chem. Int. Ed.,* 2013, **52**, 350–354.
53 G. Cucinotta, M. Perfetti, J. Luzon, M. Etienne, P. E. Car, A. Caneschi, G. Calvez, K. Bernot and R. Sessoli, Magnetic Anisotropy in a Dysprosium/DOTA Single-Molecule Magnet: Beyond Simple Magneto-Structural Correlations. *Angew. Chem. Int. Ed.,* 2012, **51**, 1606−1610.
54 J. Long, R. Vallat, R. A. S. Ferreira, L. D. Carlos, F. A. Almeida Paz, Y. Guari and J. Larionova, A bifunctional luminescent single-ion magnet: towards correlation between luminescence studies and magnetic slow relaxation processes. *Chem. Commun*. 2012, **48**, 9974-9976.
55 M. Ren, S.-S. Bao, R. A. S. Ferreira, L.-M. Zheng and L. D. Carlos, A layered erbium phosphonate in pseudo-D5h symmetry exhibiting field-tunable magnetic relaxation and optical correlation. *Chem. Commun*. 2014, **50**, 7621−7624.
56 F. Pointillart, B. Le Guennic, T. Cauchy, S. Golhen, O. Cador, O. Maury and L. Ouahab, A Series of Tetrathiafulvalene-Based Lanthanide Complexes Displaying Either Single Molecule Magnet or Luminescence-Direct Magnetic and Photo-Physical Correlations in the Ytterbium Analogue. *Inorg. Chem*. 2013, **52**, 5978−5990.
57 F. Pointillart, B. Le Guennic, S. Golhen, O. Cador, O. Maury and L. Ouahab, A redox-active luminescent ytterbium based single molecule magnet. *Chem. Commun.* 2013, **49**, 615−617.
58 F. Pointillart, B. Le Guennic, O. Cador, O. Maury and L. Ouahab, Lanthanide Ion and Tetrathiafulvalene-Based Ligand as a "Magic" Couple toward Luminescence, Single Molecule Magnets, and Magnetostructural Correlations. *Acc. Chem. Res*. 2015, *48*, 2834-2842.
59 M. Ren, S.-S. Bao, B.-W. Wang, R. A. S. Ferreira, L.-M. Zheng, L. D. Carlos, Lanthanide phosphonates with pseudo-D5h local symmetry exhibiting magnetic and luminescence bifunctional properties. *Inorg. Chem. Front*. 2015, **2**, 558-566.
60 J. Long, E. Mamontova, V. Freitas, D. Luneau, V. Vieru, L. F. Chibotaru, R. A. S. Ferreira, G. Félix, Y. Guari, L. D. Carlos and J. Larionova, Study of the influence of magnetic dilution over relaxation processes in a Zn/Dy single-ion magnet by correlation between luminescence and magnetism. *RSC Adv.*, 2016, **6**, 108810-108818.
61 K. Soussi, J. Jung, F. Pointillart, B. Le Guennic, B. Lefeuvre, S. Golhen, O. Cador, Y. Guyot, O. Maury and L. Ouahab, Magnetic and photo-physical investigations into DyIII and YbIII complexes involving tetrathiafulvalene ligand. *Inorg. Chem. Front.*, 2015, **2**, 1105-1117.
62 J. Long, Y. Guari, R. A. S. Ferreira, L. D. Carlos and J. Larionova, Recent advances in luminescent lanthanide based Single-Molecule Magnets. *Coord. Chem. Rev.*, 2018, **363**, 57-70.
63 Y. Huo, Y.-C. Chen, S.-G. Wu, J.-L. Liu, J.-H. Jia, W.-B. Chen, B.-L. Wang, Y.-Q. Zhang and M.-L. Tong, Effect of Bridging Ligands on Magnetic Behavior in Dinuclear Dysprosium Cores Supported by Polyoxometalates. *Inorg. Chem.*, 2019, **58**, 1301-1308.
64 G. Brunet, R. Marin, M. Monk, U. Resch-Genger, D. A. Galico, F. A. Sigoli, E. A. Suturina, E. Hemmer and M. Murugesu,

Exploring the dual functionality of an ytterbium complex for luminescence thermometry and slow magnetic relaxation. *Chem. Sci.*, 2019, **10**, 6799-6808.
65 J.-H. jia, Q.-W. Li, Y.-C. Chen, J.-L. Liu and M.-L. Tong, Luminescent single-molecule magnets based on lanthanides: Design strategies, recent advances and magneto-luminescent studies. *Coord. Chem. Rev.*, 2019, **378**, 365-381.
66 B. Casanovas, S. Speed, M. S. El Fallah, R. Vicente, M. Font-Bardia, F. Zinna and L. Di Bari, Chiral dinuclear Ln(III) complexes derived from S- and R-2-(6-methoxy-2-naphthyl)propionate. Optical and magnetic properties. *Dalton Trans.*, 2019, **48**, 2059-2067.
67 D.-P. Li, T.-W. Wang, C.-H. Li, D.-S. Liu, Y.-Z. Li and X.-Z. You, Single-ion magnets based on mononuclear lanthanide complexes with chiral Schiff base ligands [Ln(FTA)3L] (Ln = Sm, Eu, Gd, Tb and Dy). *Chem. Commun.*, 2010, **46**, 2929-2931.
68 X.-L. Li, C.-L. Chen, Y.-L. Gao, C.-M. Liu, X.-L. Feng, Y.-H. Gui and S.-M. Fang, Modulation of Homochiral DyIII Complexes: Single-Molecule Magnets with Ferroelectric Properties. *Chem. Eur. J.*, 2012, **18**, 14632-14637.
69 X.-L. Li, C.-L. Chen, H.-P. Xiao, A.-L. Wang, C.-M. Liu, X. Zheng, L.-J. Gao, X.-G. Yang and S.-M. Fang, Luminescent, magnetic and ferroelectric properties of noncentrosymmetric chain-like complexes composed of nine-coordinate lanthanide ions. *Dalton Trans.*, 2013, **42**, 15325-15347.
70 J. Long, J. Rouquette, J.-M. Thibaud, R. A. S. Ferreira, L. D. Carlos, B. Donnadieu, V. Vieru, L. F. Chibotaru, L. Konczewicz, J. Haines, Y. Guari and J. Larionova, A High-Temperature Molecular Ferroelectric Zn/Dy Complex Exhibiting Single-Ion-Magnet Behavior and Lanthanide Luminescence. *Angew. Chem. Int. Ed.*, 2015, **54**, 2236-2240.
71 X.-L. Li, M. Hu, Z. Yin, C. Zhu, C.-M. Liu, H.-P. Xiao and S. Fang, Enhanced single-ion magnetic and ferroelectric properties of mononuclear Dy(III) enantiomeric pairS through the coordination role of chiral ligands. *Chem. Commun.*, 2017, **53**, 3998-4001.
72 K. Wang, S. Zeng, H. Wang, J. Dou and J. Jiang, Magneto-chiral dichroism in chiral mixed (phthalocyaninato)(porphyrinato) rare earth triple-decker SMMs. *Inorg. Chem. Front.*, 2014, **1**, 167-171.
73 K. Dhbaibi, L. Favereau and J. Crassous, Enantioenriched Helicenes and Helicenoids Containing Main-Group Elements (B, Si, N, P). *Chem. Rev.*, 2019, **119**, 8846-8953.
74 L. Polavarapu Prasad, J. He, J. Crassous and K. Ruud, Absolute Configuration of C76 from Optical Rotatory Dispersion. *ChemPhysChem*, 2005**, 6**, 2535-2540.
75 J.-K. Ou-Yang, N. Saleh, G. Fernandez Garcia, L. Norel, F. Pointillart, T. Guizouarn, O. Cador, F. Totti, L. Ouahab, J. Crassous and B. Le Guennic, Improved slow magnetic relaxation in optically pure helicene-based DyIII single molecule magnets. *Chem. Commun.*, 2016, **52**, 14474-14477.
76 G. Fernandez Garcia, J. Flores Gonzalez, J.-K. Ou-Yang, N. Saleh, F. Pointillart, O. Cador, T. Guizouarn, F. Totti, L. Ouahab, J. Crassous and B. Le Guennic, Slow Magnetic Relaxation in Chiral Helicene-Based Coordination Complex of Dysprosium. *Magnetochemistry*, 2017, **3**, 2.
77 F. Pointillart, J.-K. Ou-Yang, G. Fernandez Garcia, V. Montigaud, J. Flores Gonzalez, R. Marchal, L. Favereau, F. Totti, J. Crassous, O. Cador, L. Ouahab and B. Le Guennic, Tetrathiafulvalene-Based Helicene Ligand in the Design of a Dysprosium Field-Induced Single-Molecule Magnet. *Inorg. Chem.,* 2019, **58**, 52-56.
78 M. Galland, F. Riobé, J. Ouyang, N. Saleh, F. Pointillart, V. Dorcet, B. Le Guennic, O. Cador, J. Crassous, C. Andraud, C. Monnereau and O. Maury, Helicenic Complexes of Lanthanides: Influence of the f-Element on the Intersystem Crossing Efficiency and Competition between Luminescence and Oxygen Sensitization. *Eur. J. Inorg. Chem.*, 2019, 118-125.
79 T. Hayano, T. Sakaguchi, H. Furuno, M. Ohba, H. Okawa and J. Inanaga, Characterization of Eu(III) Adsorbed onto Chitin and Chitosan by Time-resolved Laser-induced Fluorescence Spectroscopy. *Chem. Letters*, 2003, **32**, 608-609.
80 H. Furuno, T. Hayano, T. Kambara, Y. Sugimoto, T. Hanamoto, Y. Tanaka, Y. Z. Jin, T. Kagawa and J. Inanaga, Chiral rare earth organophosphates as homogeneous Lewis acid catalysts for the highly enantioselectivehetero-Diels – Alder reactions. *Tetrahedron*, 2003, **59**, 10509-10523.
81 H. Furuno, T. Kambara, Y. Tanaka, T. Hanamoto, T. Kagawa and J. Inanaga, Highly enantioselective homogeneous catalysis of chiral rare earth phosphates in the hetero-Diels–Alder reaction. *Tetrahedron Lett.*, 2003, **44**, 6129-6132.
82 H. Furuno, T. Hanamoto, Y. Sugimoto and J. Inanaga, Remarkably High Asymmetric Amplification in the Chiral Lanthanide Complex-Catalyzed Hetero-Diels−Alder Reaction: First Example of the Nonlinear Effect in ML3 System. *Org. Lett.*, 2000, **2**, 49-52.
83 S. Fukuzawa, K. Metoki and S. Esumi, Asymmetric Diels – Alder reactions in supercritical carbon dioxidecatalyzed by rare earth complexes. *Tetrahedron*, 2003, **59**, 10445-10452.
84 S. Suzuki, H. Furuno, Y. Yokoyama and J. Inanaga, Asymmetric fluorination of β-keto esters catalyzed by chiral rare earth perfluorinated organophosphates. *Tetrahedron: asymmetry*, 2006, **17**, 504-507.
85 N. Hara, M. Okazaki, M. Shizuma, S. Marumoto, N. Tajima, M. Fujiki and Y. Imai, Swapping Circularly Polarised Luminescence ofEu(III)-Binaphthyl Hybridized Luminophore with and without Oxymethylene Spacer. *ChemistrySelect*, 2017, **2**, 10317-10322,
86 N. Koiso, Y. Kitagawa, T. Nakanishi, K. Fushimi and Y. Hasegawa, Eu(III) Chiral Coordination Polymer with a Structural Transformation System. *Inorg. Chem.*, 2017, **56**, 5741-5747.
87 A. J. Jalilah, F. Asanoma and M. Fujiki, Unveiling controlled breaking of the mirror symmetry of Eu(fod)3 with α-/β-pinene and BINAP by circularly polarised luminescence (CPL), CPL excitation, and 19F-/31P{1H}-NMR spectra and Mulliken charges. *Inorg. Chem. Front.*, 2018, **5**, 2718-2733.
88 M. F. Richardson, W. F. Wagner and D. E. Sands, Rare-earth trishexafluoroacetylacetonates and related compounds. *J. Inorg. Nucl. Chem.*, 1968, **30**, 1275-1289.
89 A. Ngo Ndimba, T. Roisnel, G. Argouarch and C. Lalli, Harvesting New Chiral Phosphotriesters by Phosphorylation of BINOL and Parent Bis-phenols. *Synthesis*, 2019, **51**, 865-873.
90 G. M. Sheldrick, SHELXT – Integrated space-group and crystal-structure determination. *Acta Crystallogr., Sect. A*, 2015, **71**, 3-8.
91 G. M. Sheldrick, Crystal structure refinement with SHELXL. *Acta Crystallogr., Sect. C*, 2015, **71**, 3-8.
92 M. J. Frisch, G. W. Trucks, H. B. Schlegel, G. E. Scuseria, M. A. Robb, J. R. Cheeseman, G. Scalmani, V. Barone, B. Mennucci, G. A. Petersson, et al. Gaussian 09 Revision, A.02; Gaussian Inc.: Wallingford, CT, USA, 2009.
93 J. P. Perdew, K. Burke, M. Ernzerhof, Generalized Gradient Approximation Made Simple. *Phys. Rev. Lett.*, 1996, **77**, 3865–3868.
94 C. Adamo and V. Barone, Toward reliable density functional methods without adjustable parameters: The PBE0 model. *J. Chem. Phys.*, 1999, **110**, 6158–6170.
95 F. Weigend and R. Ahlrichs, Balanced basis sets of split valence, triple zeta valence and quadruple zeta valence quality for H to Rn: Design and assessment of accuracy. *Phys. Chem. Chem. Phys.*, 2005, **7**, 3297–3305
96 J. Tomasi, B. Mennucci and R. Cammi, Quantum Mechanical Continuum Solvation Models. *Chem. Rev.*, 2005, **105**, 2999–3093.

97 M. Cossi and V. Barone, Time-dependent density functional theory for molecules in liquid solutions. *J. Chem. Phys.*, 2001, **115**, 4708–4717.
98 R. Improta, V. Barone, G. Scalmani and M. J. A. Frisch, A state-specific polarizable continuum model time dependent density functional theory method for excited state calculations in solution. *J. Chem. Phys.*, 2006, **125**, 054103–054109.
99 M. Dolg, H. Stoll and H. Preuss, A combination of quasirelativistic pseudopotential and ligand field calculations for lanthanoid compounds. *Theor. Chim. Acta.*, 1993, **85**, 441–450.
100 G. te Velde, F. M. Bickelhaupt, E. J. Baerends, S. J. A. van Gisbergen, C. Fonseca Guerra, J. G. Snijders and T. Ziegler, Chemistry with ADF. *J. Comput. Chem.*, 2001, **22**, 931-967.
101 C. Fonseca Guerra, J. G. Snijders, G. te Velde and E. J. Baerends, Towards an order-N DFT method. *Theor. Chem. Acc.*, 1998, **99**, 391.
102 E. J. Baerends, T. Ziegler, A. J. Atkins, J. Autschbach, D. Bashford, O. Baseggio, A. Bérces, F. M. Bickelhaupt, C. Bo, P. M. Boerritger, L. Cavallo, C. Daul, D. P. Chong, D. V. Chulhai, L. Deng, R. M. Dickson, J. M. Dieterich, D. E. Ellis, M. van Faassen, A. Ghysels, A. Giammona, S. J. A. van Gisbergen, A. Goez, A. W. Götz, S. Gusarov, F. E. Harris, P. van den Hoek, Z. Hu, C. R. Jacob, H. Jacobsen, L. Jensen, L. Joubert, J. W. Kaminski, G. van Kessel, C. König, F. Kootstra, A. Kovalenko, M. Krykunov, E. van Lenthe, D. A. McCormack, A.; Michalak, M. Mitoraj, S. M.; Morton, J. Neugebauer, V. P. Nicu, L. Noodleman, V. P. Osinga, S. Patchkovskii, M. Pavanello, C. A. Peeples, P. H. T. Philipsen, D. Post, C. C. Pye, H. Ramanantoanina, P. Ramos, W. Ravenek, J. I. Rodríguez, P. Ros, R. Rüger, P. R. T. Schipper, D. Schlüns, H. van Schoot, G. Schreckenbach, J. S. Seldenthuis, M. Seth, J. G. Snijders, M. M. S. Solà, M. Swart, D. Swerhone, G. te Velde, V. Tognetti, P. Vernooijs, L. Versluis, L. Visscher, O. Visser, F. Wang, T. A. Wesolowski, E. M. van Wezenbeek, G. Wiesenekker, S. K. Wolff, T. K. Woo and A. L. Yakovlev, "ADF2017, SCM, Theoretical Chemistry, Vrije Universiteit, Amsterdam, The Netherlands, https://www.scm.com", 2017.
103 M. Ernzerhof and G. E. Scuseria, Assessment of the Perdew–Burke–Ernzerhof exchange-correlation functional. *J. Chem. Phys.*, 1999, **110**, 5029–5036.
104 E. van Lenthe and E. J. Baerends, Optimized Slater-type basis sets for the elements 1–118. *J. Comput. Chem.*, 2003, **24**, 1142-1156.
105 J. Autschbach and T. Ziegler, Calculating molecular electric and magnetic properties from time-dependent density functional response theory. *J. Chem. Phys.*, 2002, **116**, 891-896.
106 J. Autschbach, T. Ziegler, S. Patchkovskii, S. J. A. van Gisbergen and E. J. Barends Chiroptical properties from time-dependent density functional theory. II. Optical rotations of small to medium sized organic molecules. *J. Chem. Phys.*, 2002, **117**, 581-592.
107 E. van Lenthe, E. J. Baerends and J. G. Snijders, Relativistic regular two-component Hamiltonians. *J. Chem. Phys.*, 1993, **99**, 4597-4610
108 C. C. Pye and T. Ziegler, An implementation of the conductor-like screening model of solvation within the Amsterdam density functional package. *Theor. Chem. Acc.*, 1999, **101**, 396-408.
109 R. L. Martin, Natural transition orbitals. *J. Chem. Phys.*, 2003, **118**, 4775-4777.
110 G. Schreckenbach and T. Ziegler, Combined Density Functional Theory and Intrinsic Reaction Coordinate Study on the Conrotatory Ring-Opening of Cyclobutene. *J. Phys. Chem.*, 1995, **99**, 606-611.
111 S. De, D. Flambard, D. Garnier, P. Herson, P. Köhler, A. Mondal, K. Costuas, B. Gillon, R. Lescouëzec, B. Le Guennic and F. Gendron, Chem. Eur. J., 2019, **25**, 12120-12136.
112 I. Fdez. Galván, M. Vacher, A. Alavi, C. Angeli, F. Aquilante, J. Autschbach, J. J. Bao, S. I. Bokarev, N. A. Bogdanov, R. K. Carlson, L. F. Chibotaru, J. Creutzberg, N. Dattani, M. G. Delcey, S. S. Dong, A. Dreuw, L. Freitag, L. M. Frutos, L. Gagliardi, F. Gendron, A. Giussani, L. González, G. Grell, M. Guo, C. E. Hoyer, M. Johansson, S. Keller, S. Knecht, G. Kovačević, E. Källman, G. Li Manni, M. Lundberg, Y. Ma, S. Mai, J. P. Malhado, P. Å. Malmqvist, P. Marquetand, S. A. Mewes, J. Norell, M. Olivucci, M. Oppel, Q. M. Phung, K. Pierloot, F. Plasser, M. Reiher, A. M. Sand, I. Schapiro, P. Sharma, C. J. Stein, L. K. Sørensen, D. G. Truhlar, M. Ugandi, L. Ungur, A. Valentini, S. Vancoillie, V. Veryazov, O. Weser, T. A. Wesołowski, P.-Ol. Widmark, S. Wouters, A. Zech, J. P. Zobel, and R. Lindh, OpenMolcas: From Source Code to Insight. *J. Comput. Chem.,* 2019, **15**, 5925–5964.
113 B. O. Roos, P. R. Taylor and P. E. M. Siegbahn, A complete active space SCF method (CASSCF) using a density matrix formulated super-CI approach. *Chem. Phys.*, 1980, **48**, 157–173.
114 M. Douglas and N. M.; Kroll, Quantum electrodynamical corrections to the fine structure of helium. *Ann. Phys.*, 1974, **82**, 89-155.
115 B. A. Hess, Applicability of the no-pair equation with free-particle projection operators to atomic and molecular structure calculations. *Phys. Rev. A*, 1985, **32**, 756-763.
116 B. A. Hess, Relativistic electronic-structure calculations employing a two-component no-pair formalism with external-field projection operators. *Phys. Rev. A*, 1986, **33**, 3742-3748.
117 A. Wolf, M. Reiher and B. A. Hess, The generalized Douglas–Kroll transformation. *J. Chem. Phys.*, 2002, **117**, 9215-9226.
118 P.-O. Widmark, P.-A. Malmqvist and B.-O. Roos, Density matrix averaged atomic natural orbital (ANO) basis sets for correlated molecular wave functions. *Theor. Chim. Acta*, 1990, **77**, 291–306.
119 B. O. Roos, R. Lindh, P.-A Malmqvist, V. Veryazov and P.-O. Widmark, Main Group Atoms and Dimers Studied with a New Relativistic ANO Basis Set. *J. Phys. Chem. A*, 2004, **108**, 2851–2858.
120 B. O. Roos, R. Lindh, P.-A. Malmqvist, V. Veryazov and P.-O. Widmark, New Relativistic ANO Basis Sets for Transition Metal Atoms. *J. Phys. Chem. A*, 2005, **109**, 6575.
121 P.-A. Malmqvist, B. O. Roos and B. Schimmelpfennig, The restricted active space (RAS) state interactionapproach with spin–orbit coupling. *Chem. Phys. Lett.*, 2002, **357**, 230-240.
122 H. Bolvin, An Alternative Approach to the g-Matrix: Theory and Applications. *ChemPhysChem*, 2006, **7**, 1575-1589.
123 L. F. Chibotaru and L. Ungur, Ab initio calculation of anisotropic magnetic properties of complexes. I. Unique definition of pseudospin Hamiltonians and their derivation. *J. Chem. Phys.*, 2012, **137**, 064112-22.
124 M. Llunell, D. Casanova, J. Cirera, P. Alemany and S. Alvarez, S. SHAPE Program for the Stereochemical Analysis of Molecular Fragments by Means of Continuous Shape Measures and Associated Tools; Departament de Quimica Fisica, Departament de Quimica Inorganica,and Institut de Quimica Teorica i Computacional - Universitat de` Barcelona, Barcelona, Spain.
125 A. W. J. Poh, J. A. A Aguilar, A. M. Kenwright, K. Mason and D. Parker, Aggregation of Rare Earth Coordination Complexes in Solution Studied by Paramagnetic and DOSY NMR. *Chem. Eur. J.*, 2018, **24**, 16170-16175.
126 S. Denis-Quanquin, F. Riobé, M.-A. Delsuc, O. Maury and N. Giraud, Paramagnetic DOSY: An Accurate Tool for the Analysis of the Supramolecular Interactions between Lanthanide Complexes and Proteins. *Chem. Eur. J.*, 2016, **22**, 18123-18131.

127 R. Evans, Z. Deng, A. K. Rogerson, A. S. McLachlan, J. J. Richards, M. Nilsson and G. A. Morris, Quantitative Interpretation of Diffusion-Ordered NMR Spectra: Can We Rationalize Small Molecule Diffusion Coefficients? Angew. Chem. Int. Ed., 2013, **52**, 3199-3202.
128 R. Evans, G. D. Poggetto, M. Nilsson, G. A. Morris, Improving the Interpretation of Small Molecule Diffusion Coefficients. *Anal. Chem.*, 2018, **90**, 3987−3994.
129 S. Di Pietro, S. Lo Piano, L. Di Bari, Pseudocontact shifts in lanthanide complexes with variable crystal fieldparameters. *Coord. Chem. Rev.*, 2011, **255**, 2810- 2820.
130 O. Kahn, Molecular Magnetism, Wiley-VCH, Weinhem, Germany, 1993.
131 J. M. Zadrozny, M. Atanasov, A. M. Bryan, C.-Y. Lin, B. D. Rekken, P. P. Power, F. Neese, J. R. Long, Slow magnetization dynamics in a series of twocoordinate iron(II) complexes. *Chem. Sci.*, 2013, **4**, 125-138.
132 M. Feng, F. Pointillart, B. Lefeuvre, V. Dorcet, S. Golhen, O. Cador, L. Ouahab, Multiple Single-Molecule Magnet Behaviors in Dysprosium Dinuclear Complexes Involving a Multiple Functionalized TetrathiafulvaleneBased Ligand. *Inorg. Chem.*, 2015, **54**, 4021-4028.
133 O. Galangau, V. Montigaud, J. Flores Gonzalez, B. Lefeuvre, V. Dorcet, B. Le Guennic, O. Cador, L. Ouahab, F. Pointillart, N3O6versusN2O6coordinated dysprosium slow magnetic relaxationin a tetrathiafulvalene-based dinuclear complex. *Polyhedron*, **2019**, 168, 28-36.
134 B. Lefeuvre, O. Galangau, J. Flores Gonzalez, V. Montigaud, V. Dorcet, L. Ouahab, B. Le Guennic, O. Cador, F. Pointillart, Field-Induced Dysprosium Single-Molecule Magnet Based on a Redox-Active Fused 1,10-Phenanthroline-Tetrathiafulvalene-1,10-Phenanthroline Bridging Triad. *Front. Chem.*, 2018, **6**, 552-562.
135 L. T. A. Ho, L. F. Chibotaru, Intermolecular mechanism for multiple maxima in molecular dynamic susceptibility. *Phys. Rev. B*, 2018, **98**, 174418.
136 A. B. Canaj, M. K. Singh, C. Wilson, G. Rajaraman and M. Murrie, Chemical and in silico tuning of the magnetization reversal barrier in pentagonal bipyramide Dy(III) single-ion magnets. *Chem. Commun.* 2018, **54**, 8273-8276.
137 Y. Gil, L. Llanos, P. Cancino, P. Fuentealba, A. Vega, E. Spodine, D. Aravena, Effect of Second-Sphere Interactions on the Magnetic Anisotropy of Lanthanide Single-Molecule Magnets: Electrostatic Interactions and Supramolecular Contacts. *J. Phys. Chem. C* 2020, **124**, 5308-5320.
138 L. T. A. Ho, L. F. Chibotaru, Multiple relaxation times in single-molecule magnets. *Phys. Rev. B*, 2016, **94**, 104422.
139 G. Cosquer, F. Pointillart, J. Jung, B. Le Guennic, S. Golhen, O. Cador, Y. Guyot, A. Brenier, O. Maury, L. Ouahab, Alkylation Effects in Lanthanide Complexes Involving Tetrathiafulvalene Chromophores: Experimental and Theoretical Correlation between Magnetism and Near-Infrared Emission. *Eur. J. Inorg. Chem.*, 2014, 69-82.
140 G. Cosquer, F. Pointillart, S. Golhen, O. Cador and L. Ouahab, Slow Magnetic Relaxation in Condensed versus Dispersed Dysprosium(III) Mononuclear Complexes. *Chem. Eur. J.*, 2013, **19**, 7895.
141 F. Habib, P. H. Lin, J. Long, I. Korobkov, W. Wernsdorfer and M. Murugesu, The Use of Magnetic Dilution To Elucidate the Slow Magnetic Relaxation Effects of a Dy2 Single-Molecule Magnet. *J. Am. Chem. Soc.*, 2011, **133**, 8830-8833.
142 X. Yi, K. Bernot, V. Le Corre, G. Calvez, F. Pointillart, O. Cador, B. Le Guennic, J. Jung, O. Maury, V. Placide, Y. Guyot, T. Roisnel, C. Daiguebonne and O. Guillou, Unraveling the Crystal Structure of Lanthanide–Murexide Complexes: Use of an Ancient Complexometry Indicator as a Near-Infrared-Emitting Single-Ion Magnet. *Chem. Eur. J.*, 2014, **20**, 1569-1576.
143 F. Pointillart, J. Jung, R. Berraud-Pache, B. Le Guennic, V. Dorcet, S. Golhen, O. Cador, O. Maury, Y. Guyot, S. Decurtins, S.-X. Liu and L. Ouahab, Luminescence and Single-Molecule Magnet Behavior in Lanthanide Complexes Involving a Tetrathiafulvalene-Fused Dipyridophenazine Ligand. *Inorg. Chem.*, 2015, **54**, 5384-5397.
144 G. Pescitelli, L. Di Bari and N. Berova, Conformational aspects in the studies of organic compounds by electronic circular dichroism. *Chem. Soc. Rev.*, 2011, **40**, 4603-4625.
145 N. Berova, L. Di Bari and G. Pescitelli, Application of electronic circular dichroism in configurational and conformational analysis of organic compounds. *Chem. Soc. Rev.*, 2007, **36**, 914-931.
146 L. Di Bari, G. Pescitelli and P. Salvadori, Conformational Study of 2,2′-Homosubstituted 1,1′-Binaphthyls by Means of UV and CD Spectroscopy. *J. Am. Chem. Soc.*, 1999, **121**, 7998-8004.
147 S. Guy, A. Bensalah-Ledoux, A; Lambert, Y. Guillin, L. Guy and J. C. Mulatier, Chiral organic thin films: How far pulsed laser deposition can conserve chirality. *Thin Solid Films*, 2012, **520**, 6440-6445.
148 T. Kimoto, N. Tajima, M. Fujiki and Y. Imai, Control of Circularly Polarized Luminescence by Using Open- and Closed-Type Binaphtyl Derivatives with the Same Axial Chirality. *Chem. Asian J.* 2012, **7**, 2836-2841.
149 T. Kinuta, N. Tajima, M. Fujiki, M. Miyazawa and Y. Imai, Control of circularly polarized photoluminescent property via dihedral angle of binaphtyl derivatives. *Tetrahedron* 2012, **68**, 4791-4796.
150 T. Sato, N. Tajima, H. Ueno, T. Harada, M. Fujiki and Y. Imai, Binaphthyl luminophores with triphenylsilyl groups: sign inversion of circularly polarized luminescence and circular dichroism. *Tetrahedron* 2016, **72**, 7032-7038.
151 K. Binnemans, Interpretation of europium(III) spectra. *Coord. Chem. Rev.* 2015, **295**, 1-45.
152 C. Freund, W. Porzio, U. Giovanella, F. Vignali, M. Pasini, S. Destri, A. Mech, S. Di Pietro, L. Di Bari and P. Mineo, Thiophene Based Europium β-Diketonate Complexes: Effect of the Ligand Structure on the Emission Quantum Yield. *Inorg. Chem.*, 2011, **50**, 5417-5429.
153 A. Zaïm, H. Nozary, L. Guénée, C. Besnard, J.-F. Lemmonier, S. Petoud and C. Piguet, N-Heterocyclic Tridentate Aromatic Ligands Bound to [Ln(hexafluoroacetylacetonate)3] Units: Thermodynamic, Structural, and Luminescent Properties. *Chem. Eur. J.*, 2012, **18**, 7155-7168.